Continuum approach to self-similarity and scaling in morphological relaxation of a crystal with a facet

Dionisios Margetis,[1] Michael J. Aziz,[2] and Howard A. Stone[2]
[1]*Department of Mathematics, Massachusetts Institute of Technology, Cambridge, Massachusetts 02139, USA*
[2]*Division of Engineering and Applied Sciences, Harvard University, Cambridge, Massachusetts 02138, USA*
(Received 1 April 2004; revised manuscript received 5 October 2004; published 26 April 2005)

The morphological relaxation of axisymmetric crystal surfaces with a single facet below the roughening transition temperature is studied analytically for diffusion-limited (DL) and attachment-detachment-limited (ADL) kinetics with inclusion of the Ehrlich-Schwoebel barrier. The slope profile $F(r,t)$, where r is the polar distance and t is time, is described via a nonlinear, fourth-order partial differential equation (PDE) that accounts for step line-tension energy g_1 and step-step repulsive interaction energy g_3; for ADL kinetics, an effective surface diffusivity that depends on the step density is included. The PDE is derived directly from the step-flow equations and, alternatively, via a continuum surface free energy. The facet evolution is treated as a free-boundary problem where the interplay between g_1 and g_3 gives rise to a region of rapid variations of F, a boundary layer, near the expanding facet. For long times and $g_3/g_1 < O(1)$ singular perturbation theory is applied for self-similar shapes close to the facet. For DL kinetics and a class of axisymmetric shapes, (a) the boundary-layer width varies as $(g_3/g_1)^{1/3}$, (b) a universal ordinary differential equation (ODE) is derived for F, and (c) a one-parameter family of solutions of the ODE are found; furthermore, for a conical initial shape, (d) distinct solutions of the ODE are identified for different g_3/g_1 via effective boundary conditions at the facet edge, (e) the profile peak scales as $(g_3/g_1)^{-1/6}$, and (f) the change of the facet radius from its limit as $g_3/g_1 \to 0$ scales as $(g_3/g_1)^{1/3}$. For ADL kinetics a boundary layer can still be defined, with thickness that varies as $(g_3/g_1)^{3/8}$. Our scaling results are in excellent agreement with kinetic simulations.

DOI: 10.1103/PhysRevB.71.165432 PACS number(s): 68.35.Md, 61.46.+w, 61.50.Ah

I. INTRODUCTION

Advances in the fabrication of small structures and devices have stimulated interest in low-temperature kinetic processes on crystal surfaces. In most experimental situations, nanoscale solid structures are not in thermodynamic equilibrium and decay in time with a lifetime that typically scales with an Arrhenius function of the temperature T and a large power of the feature size. Strategies for skirting the lifetime limitations involve processing at ever-lower temperatures for ever-smaller feature sizes. The theoretical description of the thermodynamics, kinetics, and macroscopic evolution of surfaces at low temperatures is an area of active research.[1,2]

Every crystal surface at thermodynamic equilibrium experiences a roughening transition at a temperature T_R (Refs. 3–7) that depends on the surface orientation: for any given T, smooth or continuously curved parts of the surface have roughening transition temperature $T_R < T$ whereas macroscopic, flat regions of the surface known as facets[8] have $T_R > T$. Below T_R, the surface morphology can be described by a collection of atomically smooth terraces separated by steps; as T increases above T_R the step free energy vanishes and terraces can no longer be identified, as steps cover the entire surface, which appears rough.[9] The physical processes driving surface evolution are thus distinctly different in the two temperature regimes. In particular, below T_R surface relaxation occurs via the lateral motion of steps, which is caused by three major processes: diffusion of point defects ("adatoms") across terraces, attachment and detachment of adatoms at the step edges, and diffusion of atoms along the step edges. The latter process is not important in a broad class of problems such as the one considered here.

Theoretical studies of morphological evolution aim to describe the surface morphology at mesoscopic or macroscopic length scales (typically of the order of microns or larger) by accounting for the motion of adatoms or individual steps at smaller length scales (typically of the order of nanometers or smaller).[6,10,11] There are two different approaches for such theoretical efforts. One approach treats directly the coarse-grained surface height and slope profiles by using continuum principles such as continuum thermodynamics and mass conservation, expressed by partial differential equations (PDEs)[1,12–29] or variational formulations.[30] The advantage of this approach lies in its relative simplicity because models invoked in this category are often analytically tractable and hence amenable to simple quantitative predictions. However, such models have been criticized[28,31–33] for not correctly taking into account the discrete effects of the facet boundaries, which may be sensitive to the interaction between extremal steps of opposite sign.

The second approach primarily treats surface evolution by either mimicking the motion of many atoms via microscopic models,[34–37] or the motion of individual steps via step-flow models and kinetic simulations[19,21,32,33,38–42] in which the step motion results from the transfer of adatoms across the terraces separating steps.[43] The step-flow models provide detailed information about the surface evolution at the nanoscale, and can offer valuable input data for the improvement of the continuum models.[28,29,32,41] Nevertheless, the numerical simulations of this approach are limited in their ability to recognize universal features of surface evolution such as the scaling with the physical parameters.

We choose the former, continuum approach in this paper and focus on scaling aspects of nanostructure decay. Moti-

vated by results of kinetic simulations[32,41] and the corresponding efforts to combine discrete and continuum approaches for self-similar shapes at long times (in particular, Fig. 6 of Ref. 32), we sought to apply boundary-layer ideas to the decay problem. Our treatment transcends the previously stated[28,31,33] limitations of continuum models in the ability to predict the scaling behavior near the facet edge.

The morphological equilibration by surface diffusion of corrugated surfaces above T_R was described via a classical continuum approach over 40 years ago.[12,13] This analysis is based on the assumption that the surface free energy is a smooth function of the surface orientation, which enables the derivation of a fourth-order PDE with smooth solutions for the coarse-grained height profile. Essential in this formulation is a mass conservation equation for surface atoms, a chemical potential proportional to the curvature,[14] and a surface current proportional to the chemical potential gradient. The resulting PDE is not applicable below T_R, where facets are present, because the surface free energy is not analytic at the facet orientations.[2,4,15,16]

Systematic efforts to treat morphological evolution below T_R via continuum principles began in the mid-1980s and continue to the present.[1,17–27,29,30] In these treatments the motion of steps below the T_R of the high-symmetry, "basal" plane of the crystal is taken into account by introduction of the step density as a continuous variable, F, which is proportional to the surface slope on a scale large compared to the step separation (typically of the order of $1-10$ nm). Nonlinear PDEs have been derived for F or the height h in cases with unidirectional or bidirectional periodic surface modulations.[19–21] An essential ingredient of these equations is an analytical expression for the chemical potential of atoms at interacting step edges, which is termed the "step chemical potential,"[31,33] i.e., the change in the free energy of the system of interacting steps by the removal or addition of an atom at a step edge. Fourth-order nonlinear PDEs for F can then be derived in the case where surface diffusion is the rate-limiting process.[19,21,23] Considerable progress has been made in solving the PDEs by invoking separation of variables,[21] power series expansions,[23,24] and shape-preserving (similarity) solutions[21,23,32] that satisfy ordinary differential equations (ODEs), but further progress has been hindered by the presence of macroscopic facets.[23,27,28,30–33,41,42] In this case the solutions to the PDEs develop singularities at the facet edge, which are intimately related to the nonanalyticity of the surface free energy G as a function of the surface slope in the vicinity of the facet orientation.

In order to address mathematically the first difficulty of the singular behavior associated with the presence of facets, Spohn[23] allowed for time-dependent facet formation by treating the relevant PDE problem as a free-boundary problem. In the analysis the chemical potential associated with steps is extended continuously onto facets of unidirectional surface modulations; the PDE was solved[23,24] subject to a set of boundary conditions at the moving facet edge. This approach, though natural and not uncommon in continuum mechanics, has been criticized[31,33] for excluding the effects of step-antistep attractive interactions when steps of opposite sign bounding a facet come close to each other. However, we do not believe that such criticisms are conclusive about the limitations of continuum approaches for the following reasons: (a) From the physical and experimental standpoints, it is of interest at the meso or macroscales to find universal, scaling laws that involve physical, nondimensional parameters such as the ratio of the step interaction energy to the energy ("line tension") of an isolated step; it is unclear to what extent the details of the individual step motion matter for this purpose. (b) In many physical situations the effect of attractive step-antistep interactions can be neglected compared to other energies such as line tension that can dominate the morphological evolution, for instance, in the case with single-faceted structures such as those originating from large initial cones,[32] which consist of circular steps. (c) Spohn's analysis identifies and provides insight into the problem of using suitable "effective" continuum boundary conditions at the facet edge. We believe that issues (a) and (c), though directly amenable to a treatment by a continuum theory, have not been adequately addressed in the literature. In this paper, we report progress towards both of these issues.

Other continuum approaches[17,25,27] deal with facets via regularization of the surface free energy and application of continuum equations everywhere along the surface. A small parameter, or regulator, is introduced to smooth out the surface free energy as a function of the slope. As a result, the solutions for the slope profile are also smooth, with nearly flat extrema but no actual facets anywhere. This method has been criticized due to fundamental considerations[30,33] such as the lack of physical meaning of the regulator; furthermore, it has not been shown that the results converge with those of step kinetic simulations.[28]

Shenoy and Freund[30] circumvent the difficulty associated with the presence of facets by using a variational formulation and Fourier series expansions that replace local relations, such as that between the adatom current and the chemical potential, by coupled ODEs for the time-dependent expansion coefficients, which they solve numerically. This method appears to be consistent with Spohn's[23] treatment of facets but does not deal directly with the scaling of the solutions with the physical parameters.

In this paper we study universal, scaling aspects of morphological evolution below T_R by using a PDE, and treat facet evolution as a free-boundary problem.[23,24] We consider crystalline structures having a single facet and closed curved steps. Because of the inclusion of the line tension and the step curvature in this case, our analysis is different from Spohn's treatment[23] of surface diffusion, which focuses on unidirectional surface modulations. We are motivated by kinetic simulations[32] for initial conical shapes: the authors numerically solved a large number of coupled ODEs to show that the slope profile F has a self-similar behavior at long times, with similarity variable $rt^{-1/4}$, where r is the polar distance and t is time. Furthermore, in Ref. 32 the authors started with the coupled, step-flow equations and derived an ODE for the similarity function, but were unable to solve it uniquely. A particular feature of the simulation results that was not quantified or even noticed is the rapid change of F in a region near the facet. As we show, this region can be treated as a "boundary layer" and its width depends nontrivially on the ratio of the step interaction energy to the line tension for both DL and ADL kinetics.

We apply boundary-layer theory to quantify the scaling of the surface slope F with the ratio of step interaction energy to line tension for both DL and ADL kinetics, and also resolve the uniqueness problem for DL kinetics by giving a sufficient set of boundary conditions at the facet edge. The main ideas for pure DL kinetics were outlined recently in a letter.[29] This paper is organized as follows. In Sec. II we derive a PDE for the height $h(\mathbf{r},t)$ and height gradient $\mathbf{F}=-\nabla h$ for mixed ADL and DL kinetics, with inclusion also of the Ehrlich–Schwoebel barrier.[44,45] Specifically, in Sec. II A we start with the kinetic equations for circular steps bounding terraces below the basal plane's T_R and take the continuum limit; the resulting slope profile is axisymmetric, respects mass conservation, and satisfies a fourth-order nonlinear PDE, where the current is related to the step chemical potential gradient via an effective diffusivity which, when ADL kinetics is included, is slope-dependent. In Sec. II B we apply a continuum surface-free energy approach, relax the condition of axisymmetry and thereby derive a more general PDE for **F** that includes non-axisymmetric, single-faceted structures. In Sec. II C we formulate a boundary-value problem for pure DL kinetics and axisymmetric structures. In Sec. III we treat DL kinetics: We develop free-boundary and boundary-layer theories to describe a self-similar step density F close to the facet, find scaling with the ratio of step interaction energy to line tension, and derive a unique F by applying the boundary conditions of Sec. II C at the facet edge. In Sec. IV we address the more intricate case of scaling with the ratio of the step interaction energy to the line tension for pure ADL kinetics. We find that, although a similarity solution for the step density is then not defined in the same sense as for DL kinetics, the boundary-layer ideas still apply. In Sec. V we compare our scaling results for DL and ADL kinetics with the kinetic simulation data and find excellent agreement for four distinct scaling predictions. Finally, in Sec. VI we conclude our work with a general discussion including the possible relevance of our results to experiments.

II. CONTINUUM THEORY

In a coarse-grained continuum theory surface evolution is described by using as a continuous variable the surface height $h(\mathbf{r},t)$ or the positive surface gradient $|\nabla h|$, which is proportional to the step density, where $\mathbf{r}=(x,y)=r\hat{\mathbf{e}}_r$ is the position vector in the high-symmetry, basal plane of the crystal and t is time; see Fig. 1 for an axisymmetric shape profile $h=h(r,t)$. The height h and the surface current $\mathbf{j}$ (atoms per length per time) are related by the mass conservation equation for atoms,[46]

$$\frac{\partial h}{\partial t}+\Omega\,\nabla\cdot\mathbf{j}=0, \tag{1}$$

where Ω is the atomic volume; for axisymmetric structures $\mathbf{j}=j(r,t)\hat{\mathbf{e}}_r$. We consider surfaces with a single facet, a flat part with zero slope, and with a concave downward and sufficiently smooth shape outside the facet. We further assume that no other facets are formed during evolution; for axisymmetric structures, this assumption implies that $\partial_r h\equiv\partial h/\partial r<0$ everywhere outside the facet.

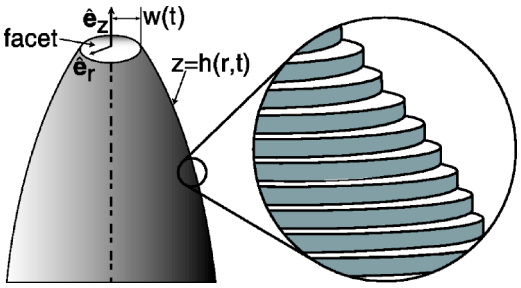

FIG. 1. View of an axisymmetric surface profile, on both the macroscale and the nanoscale where the circular steps of atomic height and the terraces separating the steps are evident. The decay of this structure is caused by the motion of steps, as the top layer periodically shrinks and collapses.

A. Kinetic equations and continuum limit for circular steps

1. First-order kinetics

We start with the kinetic formulation of Ref. 32, largely for completeness, though we modify it slightly to include the Ehrlich–Schwoebel barrier,[44,45] which refers to an increased barrier for adatom attachment and detachment to a descending step. In addition, we indicate a subtlety in the derivation of the step chemical potential, which has apparently been overlooked. We consider axisymmetric crystal surfaces characterized by N ($N\gg 1$) interacting, concentric circular steps of the same step height a, separated by flat terraces parallel to the basal plane (see Fig. 1); the ith terrace lies between the ith and $(i+1)$th step, in the region $r_i<r<r_{i+1}$, where r is the polar distance, $i=0,1,\ldots,N-1$, and $i=0$ corresponds to the facet, $r_0=0<r<r_1$. It is further assumed that surface evolution is limited by the diffusion of adatoms across terraces,[43] as well as by the attachment and detachment of atoms at the step edges, while no material is deposited on the surface from above. Other transport processes such as volume (bulk) diffusion, evaporation-condensation, and diffusion along the step edges are neglected.

The adatom concentration $c_i(r,t)$ on the ith terrace satisfies the diffusion equation, $\partial c_i/\partial t=D_s\nabla^2 c_i(r,t)$, where D_s is the surface diffusivity which is assumed to be a scalar constant. In the quasistatic approximation the time derivative in the diffusion equation is neglected,[47] $\partial c_i/\partial t\approx 0$, and $c_i(r,t)$ thus satisfies the Laplace equation, $\nabla^2 c_i=0$, where the time dependence of c_i enters only implicitly through the boundary conditions at the step edges. Hence, $c_i(r,t)=A_i\ln r+B_i$ for $r_i<r<r_{i+1}$, where A_i and B_i depend only on time. By introducing the adatom current $J_i(r,t)$ on the ith terrace,

$$J_i(r,t)\equiv -D_s\frac{\partial c_i}{\partial r}=-D_s\frac{A_i(t)}{r},\quad r_i<r<r_{i+1}, \tag{2}$$

the balance of adatoms at the steps bounding the ith terrace is expressed by[48]

$$-J_i(r_i,t)=k_u[c_i(r_i,t)-C_i^{eq}], \tag{3a}$$

$$J_i(r_{i+1},t) = k_d[c_i(r_{i+1},t) - C_{i+1}^{eq}], \tag{3b}$$

where C_i^{eq} is the equilibrium concentration of atoms in the vicinity of the ith step, k_u is the rate coefficient for attachment-detachment from a terrace to an up-step edge, and k_d is the rate coefficient for attachment-detachment from a terrace to a down-step edge; note that $k_d < k_u$ for a positive Ehrlich-Schwoebel barrier. A_i and B_i can thus be determined in terms of r_i and r_{i+1}, e.g.,

$$A_i = \frac{C_i^{eq} - C_{i+1}^{eq}}{\ln(r_i/r_{i+1}) - D_s(1/k_u r_i + 1/k_d r_{i+1})}, \tag{4}$$

while the B_i are not needed for our purposes. The equilibrium concentration C_i^{eq} is related to the step chemical potential μ_i of the ith step by[32,49]

$$C_i^{eq} = c_s e^{\mu_i/k_B T} \sim c_s\left(1 + \frac{\mu_i}{k_B T}\right), \tag{5}$$

where k_B is Boltzmann's constant, T is the absolute temperature, c_s is the atom equilibrium concentration at an isolated straight step, and $k_B T \gg |\mu_i|$ for most experimental situations.[50]

The current $J_i(r,t)$ is thus expressed in terms of the step chemical potential μ_i via Eqs. (2), (4), and (5) as

$$J_i(r,t) = -\frac{D_s c_s}{k_B T}\frac{1}{r}\frac{\mu_{i+1} - \mu_i}{\ln(r_{i+1}/r_i) + D_s(1/k_u r_i + 1/k_d r_{i+1})} \tag{6}$$

for $r_i < r < r_{i+1}$. For pairwise, short-ranged, repulsive step interactions $V(r_i, r_{i+1})$ between the ith and $(i+1)$th steps, μ_i is given by[32]

$$\mu_i = \frac{\Omega g_1}{r_i} + \frac{\Omega}{2\pi a r_i}\frac{\partial[V(r_i,r_{i+1}) + V(r_{i-1},r_i)]}{\partial r_i}; \tag{7}$$

the step "stiffness" $g_1 a$ (energy/length) is the energy per unit length of an isolated step (line tension) plus its second derivative with respect to surface orientation, and a is the step height. By adopting the formula for the interactions of concentric circular steps of the same sign,[51]

$$V(r_i, r_{i+1}) = 2\pi(\breve{g}_3 a^2)\frac{r_i r_{i+1}}{(r_i + r_{i+1})(r_{i+1} - r_i)^2}, \tag{8}$$

where $\breve{g}_3$ (energy/length) is the interaction energy per unit length of the ith step, the step chemical potential μ_i is calculated to be[52]

$$\mu_i = \frac{\Omega g_1}{r_i} + \Omega\breve{g}_3 a\left\{\frac{2r_{i+1}}{r_{i+1}+r_i}\frac{1}{(r_{i+1}-r_i)^3} - \frac{2r_{i-1}}{r_i + r_{i-1}}\frac{1}{(r_i - r_{i-1})^3} + \frac{1}{r_i}\left[\left(\frac{r_{i+1}}{r_{i+1}+r_i}\right)^2\frac{1}{(r_{i+1}-r_i)^2} + \left(\frac{r_{i-1}}{r_i + r_{i-1}}\right)^2\frac{1}{(r_i - r_{i-1})^2}\right]\right\}. \tag{9}$$

The time dependence of each step position, $r_i = r_i(t)$, is dictated by the mass-balance equation

$$\dot{r}_i(t) = \frac{\Omega}{a}[J_{i-1}(r_i,t) - J_i(r_i,t)], \tag{10}$$

where throughout this paper the dot on top of a symbol denotes the time derivative. The system of discrete differential equations (10) with Eqs. (6)–(9) and the initial condition of given $r_i(0)$ can be solved numerically.[32] Once $r_i(t)$ are determined, the step density $F_i(t)$ corresponding to the ith terrace is calculated by

$$F_i(t) = \frac{a}{r_{i+1} - r_i}. \tag{11}$$

A few words are in order about the distinction of pure DL from pure ADL kinetics on the basis of the kinetic equations. By inspection of Eq. (6), the behavior of the adatom current, $J_i(r,t)$, in i and r depends on the interplay between the two terms in the denominator, e.g., the $\ln(r_{i+1}/r_i)$ term and the $D_s[(k_u r_i)^{-1} + (k_d r_{i+1})^{-1}]$ term. If the first term dominates, the adatom current is sensitive to *space* variations of the step chemical potential, $(\mu_{i+1} - \mu_i)/(r_{i+1} - r_i)$; this case corresponds to pure DL kinetics as diffusion across terraces is the rate-limiting process, and the continuum counterpart of $J_i(r,t)$ equals a constant times the gradient of the step chemical potential; see Eq. (21) below. In contrast, for ADL-dominated kinetics the term $\ln(r_{i+1}/r_i)$ is negligible and the adatom current is sensitive to *step* variations of the step chemical potential, $(\mu_{i+1} - \mu_i)/[(i+1) - i]$; thus, the continuum adatom current is related to the gradient of the step chemical potential via an effective surface diffusivity inversely proportional to the step density; see Eq. (22) below.

A relation that is useful in the next section where the continuum limit is considered follows by differentiation of the step density $F_i(t)$, Eq. (11), with respect to time t using Eq. (10):

$$\frac{dF_i}{dt} = -a\frac{\dot{r}_{i+1} - \dot{r}_i}{(r_{i+1} - r_i)^2} = \Omega\frac{q_{i+1} - p_i}{r_{i+1} - r_i}, \tag{12}$$

where

$$q_i = \frac{J_i(r_i,t) - J_{i-1}(r_i,t)}{r_i - r_{i-1}}, \quad p_i = \frac{J_i(r_i,t) - J_{i-1}(r_i,t)}{r_{i+1} - r_i}. \tag{13}$$

We note that, by virtue of the quasistatic assumption [Eq. (2)], the values of the adatom current at the step edges bounding the ith terrace are related by $r_{i+1}J_i(r_{i+1},t) = r_i J_i(r_i,t)$. Hence,

$$q_i = \frac{1}{r_i}\frac{r_i J_i(r_i,t) - r_{i-1}J_{i-1}(r_{i-1},t)}{r_i - r_{i-1}}, \tag{14a}$$

$$p_i = \frac{1}{r_i}\frac{r_i J_i(r_i,t) - r_{i-1}J_{i-1}(r_{i-1},t)}{r_{i+1} - r_i}. \tag{14b}$$

For separation distances that vary slowly in i, $r_{i+1} - r_i \approx r_i - r_{i-1}$ which yields $p_i \approx q_i$.[53] Equations (14) are used in the next section; we recognize that for $r_{i+1} - r_i \to 0$ their right-hand sides become the divergence of the continuous surface current $\mathbf{j}(r,t) = \hat{\mathbf{e}}_r j(r,t)$.

2. Continuum limit

We next take the continuum limit of Eq. (10) with emphasis on the structure of the equations involved, and not on the conditions of our approximations. In the continuum limit outside the facet, r_{i+1} and r_i are presumed to approach any distance $\tilde{r}_i=\tilde{\lambda}r_{i+1}+(1-\tilde{\lambda})r_i$, where $0\leqslant\tilde{\lambda}\leqslant 1$; $\tilde{r}_i$ becomes the polar distance (independent variable) r, and the step number i ($i=0,1,\ldots,N-1$) may thus vary for fixed r. The continuum step density $F(r,t)$, surface current $j(r,t)$, and step chemical potential $\mu(r,t)$ are considered as the limits for $r_{i+1}-r_i\to 0$ of the piecewise continuous functions $\tilde{F}(r,t)=F_i(t)$, $\tilde{J}(r,t)=J_i(\tilde{r}_i,t)$, and $\tilde{\mu}(r,t)=\mu_i(t)$ which are defined in each interval $r_i<r<r_{i+1}$; in the limit $r_{i+1}-r_i\to 0$ these functions are presumed to reduce to continuous functions that are also smooth in r along the sloping surface outside the facet. Necessary conditions for the validity of these assumptions are (i) $r_{i+1}-r_i\ll r_i$,[53] i.e.,

$$\frac{a}{r_iF_i}\ll 1, \tag{15}$$

and (ii) $r_{i+1}-r_i\ll L$, where L is the length over which the step density varies. If these conditions are violated, terms that account for the "discreteness" of the step motion must be retained in the continuum equations.

It follows that the difference terms in Eqs. (12)–(14) are replaced by suitable derivatives. For example, from Eq. (14a) the continuum limit of q_i is the divergence of $\mathbf{j}=j(r,t)\hat{\mathbf{e}}_r$, $\nabla\cdot\mathbf{j}=(1/r)(\partial/\partial r)(rj)$; Eq. (12) thus becomes

$$\frac{\partial F}{\partial t}=\Omega\frac{\partial}{\partial r}\nabla\cdot\mathbf{j}. \tag{16}$$

Because $F=|\nabla h|=-\partial_r h$ is the step density, where $\partial_r h<0$, this equation is readily integrated to give

$$\frac{\partial h}{\partial t}=-\Omega\nabla\cdot\mathbf{j}+K(t). \tag{17}$$

Equation (1), the usual continuum mass-conservation statement without deposition of material, is recovered for $K(t)\equiv 0$.

The surface current $j(r,t)$ can be expressed as the gradient of the step chemical potential $\mu(r,t)$ from Eq. (6). By defining $\delta r_i=r_{i+1}-r_i$, and making the approximations

$$\ln\frac{r_i}{r_{i+1}}\sim-\frac{\delta r_i}{r_i},\quad \frac{1}{r_i}+\frac{1}{r_{i+1}}\sim\frac{2}{r_i}, \tag{18}$$

and $(\mu_{i+1}-\mu_i)/\delta r_i\sim\partial\mu/\partial r$, we readily obtain

$$j(r,t)=-\frac{c_s}{k_BT}\frac{D_s}{1+mF}\frac{\partial\mu}{\partial r} \tag{19}$$

in the continuum limit, where the parameter m is defined by

$$m=\frac{2D_s}{ka},\quad \frac{1}{k}=\frac{1}{2}\left(\frac{1}{k_u}+\frac{1}{k_d}\right), \tag{20}$$

and $F_i=a/\delta r_i\sim F$ by Eq. (11). Equation (19) has the form $\mathbf{j}=-(c_s\mathcal{D}_s/k_BT)\nabla\mu$, where $\mathcal{D}_s=D_s(1+mF)^{-1}$ is an effective surface diffusivity that depends on the step density when $m\neq 0$. Note that the effect of the Ehrlich–Schwoebel barrier enters here implicitly via the effective attachment-detachment rate coefficient k, which is the harmonic average of the rate coefficients k_u and k_d. For DL kinetics, where $mF\ll 1$, Eq. (19) becomes

$$j(r,t)=-\frac{c_sD_s}{k_BT}\frac{\partial\mu}{\partial r}\quad\text{(DL kinetics)}, \tag{21}$$

whereas for ADL kinetics, $mF\gg 1$, the respective equation is

$$j(r,t)=-\frac{c_ska}{k_BT}\frac{1}{F}\frac{\partial\mu}{\partial r}\quad\text{(ADL kinetics)}. \tag{22}$$

We obtain an additional relation between $\mu(r,t)$ and $F(r,t)$ by using Eq. (9). In order to simplify this equation we use the formulas $r_{i+1}=r_i+aF_i^{-1}$ and $r_{i-1}=r_i-aF_{i-1}^{-1}$, along with condition (15), and thus establish the approximations $r_{i+1}^2/(r_i+r_{i+1})^2\sim\frac{1}{4}\sim r_{i-1}^2/(r_i+r_{i-1})^2$ and

$$\frac{2r_ir_{i\pm1}}{r_i+r_{i\pm1}}\sim\left(r_i\pm\frac{a}{F_i}\right)\left(1\mp\frac{a}{2r_iF_i}\right)\sim r_i\pm\frac{a}{2F_i}. \tag{23}$$

Hence, Eq. (9) reduces to

$$\mu_i\sim\frac{\Omega g_1}{r_i}+\Omega\breve{g}_3a\left[\frac{F_i^2+F_iF_{i-1}+F_{i-1}^2}{a^3}(F_i-F_{i-1})+\frac{3}{4}\frac{1}{r_i}\frac{F_i^2+F_{i-1}^2}{a^2}\right]. \tag{24}$$

In the formal limit $r_i-r_{i-1}\to 0$, F_{i-1} is replaced by F_i in all terms on the right-hand side of this equation, with the exception of the difference F_i-F_{i-1}. For this last term we use

$$F_{i-1}=F_i-(\delta r_i)\frac{F_i-F_{i-1}}{\delta r_i}\sim F-\frac{a}{F}\frac{\partial F}{\partial r}, \tag{25}$$

to obtain

$$\mu(r,t)=\frac{\Omega g_1}{r}+\Omega\tilde{g}_3\frac{1}{r}\frac{\partial}{\partial r}(rF^2), \tag{26}$$

where $\tilde{g}_3=\frac{3}{2}(\breve{g}_3/a)$, with dimensions energy/(length)^2; $\tilde{g}_3$ here is defined such that it is proportional to the interaction energy per unit area of a step projected on the vertical plane.

The combination of Eqs. (16), (19), and (26) yields an evolution equation for $F=-\partial_r h$,

$$\frac{1}{B}\frac{\partial F}{\partial t}=\frac{\partial}{\partial r}\frac{1}{r}\frac{\partial}{\partial r}\frac{1}{r}\left(\frac{1}{1+mF}\right)-\frac{\tilde{g}_3}{g_1}\frac{\partial}{\partial r}\frac{1}{r}\frac{\partial}{\partial r}\times\left[\frac{r}{1+mF}\frac{\partial}{\partial r}\frac{1}{r}\frac{\partial}{\partial r}(rF^2)\right], \tag{27}$$

where the single material parameter in the development

$$B=\frac{c_sD_s\Omega^2g_1}{k_BT} \tag{28}$$

has dimensions (length)^4/time. A PDE of the same structure as Eq. (27) here is also given in Ref. 32 in terms of the step chemical potential [see their Eq. (31)]. Consistent with our

derivation and condition (15), Eq. (27) ceases to be valid in regions where the (discrete) step density F_i becomes of the order of a/r_i. This situation arises very close to the facet because the continuous slope F vanishes identically on the facet, and F_i becomes vanishingly small in the vicinity of the top step (see Sec. II C below). A PDE for the height profile, $h=h(r,t)$, is derived by combining for $K(t)=0$ Eqs. (17), (19), and (26):

$$\frac{1}{B}\frac{\partial h}{\partial t} = -\frac{1}{r}\frac{\partial}{\partial r}\frac{1}{r}\left(\frac{1}{1+m|\partial_r h|}\right) + \frac{\tilde{g}_3}{g_1}\frac{1}{r}\frac{\partial}{\partial r} \times \left\{\frac{1}{1+m|\partial_r h|}\left[r\frac{\partial^2}{\partial r^2} + \frac{\partial}{\partial r} - \frac{1}{r}\right]\left(\frac{\partial h}{\partial r}\right)^2\right\}. \quad (29)$$

Note that the effect of step permeability,[51] in which atoms traverse the steps without attaching and detaching to and from the step edges, has been claimed[32] to be taken into account effectively via a redefinition of the parameter $m=2D_s/(ka)$ at long times; specifically, the parameter k, which is associated to the attachment and detachment rate coefficients, is replaced by $k+2p$ where p is the permeability rate coefficient.

B. A general continuum surface-free energy approach

In this section we derive an evolution equation for the height profile, $h=h(\mathbf{r},t)$, and the gradient profile, ∇h, directly from continuum surface-free energy considerations for crystal shapes with a single facet by relaxing the assumption of axisymmetry of Sec. II B. Throughout this analysis, the position vector $\mathbf{r}=(x,y)$ and the gradient $\nabla=(\partial/\partial x,\partial/\partial y)$ are defined on the basal plane. The starting point is the mass conservation equation for atoms, Eq. (1). The surface current $\mathbf{j}(\mathbf{r},t)$ is the product of the areal density (surface concentration) c_s and the drift velocity, which is the product of the effective mobility of atoms, $\mathcal{D}_s/k_BT$, and the driving force, namely, the negative gradient of the step chemical potential $\mu(\mathbf{r},t)$. In the case with combined DL and ADL kinetics the effective surface diffusivity is taken to be $\mathcal{D}_s=D_s(1+m|\nabla h|)^{-1}$. This relation results from generalizing Eq. (19) from the step-flow model to include non-axisymmetric profiles consisting of closed steps with spacing small compared to (i) their local radius of curvature, and (ii) the length over which the step density varies:

$$\mathbf{j} = -\frac{c_s}{k_BT}\frac{D_s}{1+m|\nabla h|}\nabla\mu; \quad (30)$$

c_s is a constant and D_s is taken to be a scalar constant. We have made the approximation that $\mathbf{j}$ is parallel to $\nabla\mu$ which, we note, is valid for a restricted set of geometries and $m|\nabla h|$.[54] Equation (1) becomes

$$\frac{\partial h}{\partial t} = \frac{c_s D_s \Omega}{k_BT}\nabla\cdot\left(\frac{1}{1+m|\nabla h|}\nabla\mu\right). \quad (31)$$

A relation between the variables μ and h is obtained by invoking the surface free energy per unit projected area, G, which we take as azimuthally isotropic. A common expression for the G of vicinal surfaces below T_R assumes that G is a concave upward, nonanalytic function of ∇h,[1,2,16,55,56]

$$G(|\nabla h|) = g_0 + g_1|\nabla h| + \frac{1}{3}g_3|\nabla h|^3. \quad (32)$$

The g_0 term accounts for the surface free energy per unit projected area of the basal plane. The g_1 term is the energy for creating an isolated step (line tension). The g_3 term represents pairwise step interactions, including entropic repulsions due to step edge fluctuations, such as elastic dipole-dipole interactions.[1] Here we consider only repulsive step interactions, $g_3>0$, and define g_3 as multiplied by a factor $\frac{1}{3}$ in Eq. (32) for later algebraic convenience. The coefficients g_0, g_1 and g_3 are temperature dependent. Higher-order terms $O(|\nabla h|^n)$ for G $(n\geq 4)$, which may originate from quadrupole-dipole or other multipole interactions,[57] are neglected in Eq. (32). As discussed in Refs. 22 and 55, the existence of facets is analogous to a thermodynamic phase separation, and is in principle described by nonconvex surface free energies per projected area, such as those with a double-well form. Here we limit ourselves to single-faceted structures with a concave downward, smooth shape outside the facet; Eq. (32) then suffices for our purposes because the crystal shape near equilibrium is related to the surface free energy via a Legendre transform.[2,58,59]

The step chemical potential is obtained by considering the variations of the surface free energy with respect to the height gradient, $\nabla h=(h_x,h_y)$,[14,16,21]

$$\mu = \frac{\Omega}{a}\nabla\cdot\mathbf{N}, \quad (33)$$

where the vector quantity $\mathbf{N}$ is defined by[60]

$$\mathbf{N} = -a\left(\frac{\partial G}{\partial h_x}\hat{\mathbf{e}}_x + \frac{\partial G}{\partial h_y}\hat{\mathbf{e}}_y\right) \quad (34)$$

denoting $h_v=\partial h/\partial v$ for $v=x,y$. Mathematically, the introduction of $\mathbf{N}$ facilitates the expression of the boundary conditions at the facet edge, as described in the next section. The physical meaning of $\mathbf{N}$ stems from the observation that $(dl)\hat{\boldsymbol{\eta}}\cdot\mathbf{N}$ expresses the energy of a step of length dl, where $\hat{\boldsymbol{\eta}}=-\nabla h/|\nabla h|$ is the unit vector normal to the step and parallel to the basal plane that points outwards the closed curve of the step shape; for axisymmetric shapes, $\hat{\boldsymbol{\eta}}=\hat{\mathbf{e}}_r$. It follows that

$$\mathbf{N} = -ag_1\left[\left(\frac{\nabla h}{|\nabla h|}\right) + \frac{g_3}{g_1}(|\nabla h|\nabla h)\right] \quad (35)$$

and

$$\mu = -\Omega g_1\left[\nabla\cdot\left(\frac{\nabla h}{|\nabla h|}\right) + \frac{g_3}{g_1}\nabla\cdot(|\nabla h|\nabla h)\right]. \quad (36)$$

Equations (33)–(36) are valid outside the facet.

The evolution equation for the height $h(\mathbf{r},t)$ follows from Eqs. (31) and (36):

$$\frac{\partial h}{\partial t} = -B\nabla\cdot\left\{\frac{1}{1+m|\nabla h|}\left[\nabla\nabla\cdot\left(\frac{\nabla h}{|\nabla h|}\right) + \frac{g_3}{g_1}\nabla\nabla\cdot(|\nabla h|\nabla h)\right]\right\}, \tag{37}$$

where B is defined by Eq. (28); see also Ref. 61. Because of the approximation underlying Eq. (30), Eq. (37) does not fully account for terrace adatom currents parallel to steps. A nonlinear PDE for the gradient profile $\mathbf{F}=-\nabla h$ is derived by applying the gradient operator, ∇, on both sides of Eq. (37):

$$\frac{\partial \mathbf{F}}{\partial t} = -B\nabla\nabla\cdot\left\{\frac{1}{1+m|\mathbf{F}|}\left[\nabla\nabla\cdot\left(\frac{\mathbf{F}}{|\mathbf{F}|}\right) + \frac{g_3}{g_1}\nabla\nabla\cdot(|\mathbf{F}|\mathbf{F})\right]\right\}. \tag{38}$$

A comparison of Eqs. (37) and (38) with Eqs. (29) and (27) for axisymmetric shapes with $h=h(r,t)$ and $\mathbf{F}=-\hat{\mathbf{e}}_r\partial_r h$ shows that

$$g_3 = \tilde{g}_3 = \frac{3}{2}\frac{\check{g}_3}{a}, \tag{39}$$

where $\check{g}_3$ is introduced in Eq. (8).

Equation (37) or (38) must be supplemented with suitable initial and boundary conditions. As an illustration of the continuum principles involved in setting up a possible set of such conditions, we formulate an axisymmetric boundary-value problem for DL kinetics below.

C. Boundary-value problem for DL kinetics with axisymmetry

We consider DL kinetics and axisymmetric crystalline surfaces with height profile $h(r,t)$ and slope profile $F(r,t)$ (see Fig. 1). In this case the diffusion of adatoms across terraces is the rate-limiting process; the harmonic average, k, of the attachment-detachment rate coefficients k_u and k_d and the surface diffusivity D_s thus satisfy the condition $D_s \ll ka$, so that we can take $m=0$ in Eq. (27). The slope profile F therefore satisfies the nonlinear PDE

$$\frac{1}{B}\frac{\partial F}{\partial t} = \frac{3}{r^4} - \frac{g_3}{g_1}\frac{\partial}{\partial r}\nabla^2\left[\frac{1}{r}\frac{\partial}{\partial r}(rF^2)\right] = \frac{3}{r^4} - \frac{g_3}{g_1}\left(\frac{\partial^4 F^2}{\partial r^4} + \frac{2}{r}\frac{\partial^3 F^2}{\partial r^3} - \frac{3}{r^2}\frac{\partial^2 F^2}{\partial r^2} + \frac{3}{r^3}\frac{\partial F^2}{\partial r} - \frac{3}{r^4}F^2\right). \tag{40}$$

We treat facet evolution as a free-boundary problem:[23] we recognize that there is an expanding facet for $r<w(t)$, where $F=0$, and this facet connects smoothly with the rest of the profile for $r>w(t)$; here, $w=w(t;g_3/g_1)$ is the facet radius, a monotonically increasing function of time. We need to supplement Eq. (40) with an initial condition and with boundary conditions at $r=\infty$, where the slope profile approaches its initial values, and at the moving boundary $r=w$ of the facet. The unknown functions are (a) the slope F, which in principle requires four boundary conditions because it satisfies a fourth-order PDE, Eq. (40), (b) the facet radius, $w(t)$, and (c) the facet height $h_f(t)$. Hence, we seek six boundary conditions for these quantities.

Initially ($t=0$) the surface has a single facet for $r<W$ and is concave downward and smooth with negative slope for $r>W$, where $W=w(0)$ is the initial facet radius. It follows from Eq. (40) that no other facets are formed during evolution. At times $t>0$,

$$F(r,t) = 0, \quad r < w(t). \tag{41}$$

The requisite initial condition is expressed in terms of a given function $H(r)$ as

$$h(r,t=0) = H(r), \tag{42}$$

where the facet is flat,

$$F(r,0) = -H'(r) = 0, \quad 0 \leqslant r < W, \tag{43a}$$

and outside the facet the shape is smoothly and monotonically varying,

$$F(r,0) = -H'(r) > 0, \quad r > W. \tag{43b}$$

We next describe a set of boundary conditions at $r=w$ and $r=\infty$; to obtain some of these conditions at $r=w$ we exploit the structure of Eqs. (1), (30), and (33) for $m=0$. The resulting conditions suffice to provide a unique solution to Eq. (40).

A condition at the facet edge is that of slope continuity: F vanishes on the facet, by definition of the facet, and varies continuously to the surface slope outside the facet,

$$F(w,t) = 0. \tag{44}$$

This condition is consistent with the results of kinetic simulations[32,62] for an initial conical shape, and also agrees with the requirement of local equilibrium.[2,63]

A second boundary condition imposes continuity of the surface current at the facet edge, which is dictated by mass conservation. By Eqs. (19) and (26) of Sec. II A or Eqs. (30) and (36) of Sec. II B for $m=0$, the surface current outside the facet is

$$j(r,t) = \frac{c_s D_s \Omega g_1}{k_B T}\left[\frac{1}{r^2} + \frac{g_3}{g_1}\left(\frac{F^2}{r^2} - \frac{1}{r}\frac{\partial F^2}{\partial r} - \frac{\partial^2 F^2}{\partial r^2}\right)\right]. \tag{45}$$

The current on the facet, $\mathbf{j}_f = j_f(r,t)\hat{\mathbf{e}}_r$, follows by integrating the mass conservation equation, $\dot{h}_f + \Omega\nabla\cdot\mathbf{j}_f = 0$, where $h_f(t)$ is the facet height. Because axisymmetry requires that $j_f(0,t)=0$, we find

$$j_f(r,t) = -\frac{\dot{h}_f r}{2\Omega}, \quad r < w. \tag{46}$$

By equating the right-hand sides of Eqs. (45) and (46) at $r=w$, and using Eq. (44), we obtain the condition

$$1 - \frac{g_3}{g_1} w\left[(F^2)_r + w(F^2)_{rr}\right]\big|_{r=w} = -\frac{\dot{h}_f w^3}{2B}, \tag{47}$$

where $(F^2)_r \equiv \partial F^2/\partial r$.

The surface height $h=h(r,t)$ is also continuous at the facet edge,

$$h_f(t) = h(r = w^+, t). \tag{48}$$

Differentiation with respect to t of both sides of Eq. (48) gives

$$\dot{h}_f(t) = \frac{dh(w(t),t)}{dt} = \left.\frac{\partial h}{\partial t}\right|_{r=w^+} - \dot{w}F(w,t). \tag{49}$$

The value of $(\partial h/\partial t)$ as $r \to w^+$ is related to the slope F and its spatial derivatives by Eq. (29) for $m=0$, where again we use $F=0$ at $r=w^+$:

$$\left.\frac{\partial h}{\partial t}\right|_{r=w^+} = B\left\{\frac{1}{w^3} + \frac{g_3}{g_1}\left[-\frac{1}{w^2}(F^2)_r + \frac{2}{w}(F^2)_{rr} + (F^2)_{rrr}\right]\right|_{r=w}\Bigg\}. \tag{50}$$

Equation (49) therefore yields a third boundary condition,

$$1 + \frac{g_3}{g_1} w[-(F^2)_r + 2w(F^2)_{rr} + w^2(F^2)_{rrr}]|_{r=w} = \frac{\dot{h}_f w^3}{B}. \tag{51}$$

Before we give the rest of the conditions at $r=w$, we turn our attention to the behavior of F at $r=\infty$, where by Eq. (43b) we have the possible asymptotic formulas

$$F \sim -H'(r), \tag{52a}$$

$$\frac{\partial F}{\partial r} \sim -H''(r), \quad r \to \infty, \tag{52b}$$

for some class of initial profiles $H(r)$ and $g_3/g_1 \leqslant O(1)$. For instance, Eqs. (52) are expected to be satisfied for an initial conical shape, $-H'(r)=\text{const}$. By virtue of Eq. (40), the correction to the leading term given in Eq. (52a) satisfies a fourth-order PDE which, when linearized about the slope profile as $r \to \infty$, can only admit two independent, decaying exponentials as solutions for $r \to \infty$; hence, formulas (52) are interpreted as describing two independent conditions at ∞, while further differentiations with respect to r do not add any new conditions. In the special case with a conical initial shape, $H(r)=-r$, these asymptotic formulas amount to the conditions

$$F \to 1, \quad \frac{\partial F}{\partial r} \to 0, \quad r \to \infty. \tag{53}$$

We now check whether total mass conservation can yield any additional conditions at $r=\infty$. Integration in $\mathbf{r}$ of $(\partial h/\partial t) = -\Omega \nabla \cdot \mathbf{j}$ gives

$$\frac{d}{dt}\int_0^\infty dr r h(r,t) = -\Omega \int_0^\infty dr \frac{\partial}{\partial r}(rj). \tag{54}$$

Because $j(0,t)$ is finite, the right-hand side of this equation vanishes if

$$rj(r,t) \to 0 \quad \text{as } r \to \infty. \tag{55}$$

From Eqs. (45) and (52), the last condition imposes a constraint on the initial profile:

$$\frac{H'(r)^2}{r} - 2[H'(r)H''(r) + H''(r)^2 + H'(r)H'''(r)] \to 0 \tag{56}$$

as $r \to \infty$. Hence, Eq. (55) does not add any new boundary condition.

Equations (44), (47), (51), and (52) form a set of five conditions within our continuum approach. As noted above, we need six conditions. In order to provide the missing condition for $F(r,t)$, $w(t)$ and $h_f(t)$ we extend continuously onto the facet[23] the step chemical potential defined by Eq. (26) outside the facet as

$$\mu(r,t) = \Omega g_1\left[\frac{1}{r} + \frac{g_3}{g_1}\left(\frac{F^2}{r} + \frac{\partial F^2}{\partial r}\right)\right], \quad r > w. \tag{57}$$

Our setting, where line tension matters, is different from the original analysis given by Spohn.[23] We implement the continuous extension onto the facet of the variable μ by exploiting the relation between the surface current $\mathbf{j}$ and μ, i.e., $\mathbf{j} = -(c_s D_s/k_B T)\nabla\mu$. The extended step chemical potential, $\mu_f(r,t)$, is thus defined by

$$\mathbf{j}_f = \hat{\mathbf{e}}_r j_f(r,t) = -\hat{\mathbf{e}}_r \frac{B}{\Omega^2 g_1}\frac{\partial \mu_f}{\partial r}. \tag{58}$$

We emphasize that, being a mathematical construct, μ_f is neither the adatom chemical potential on the facet nor the layer chemical potential[31,33] of the topmost atomic layer. We solve for μ_f by using Eq. (46) and integrating (58):

$$\mu_f(r,t) = \frac{\Omega g_1}{4B}[\dot{h}_f r^2 + b(t)], \quad r < w, \tag{59}$$

where $b(t)$ is an as yet undetermined function of time. The continuity relation

$$\mu_f(w,t) = \mu(w^+,t), \tag{60}$$

after enforcing Eq. (44), is therefore equivalent to

$$\frac{\dot{h}_f w^3}{B} = 4\left[1 + \frac{g_3}{g_1} w(F^2)_r\right]\Bigg|_{r=w} - \frac{wb}{B}. \tag{61}$$

Equations (44), (47), (51), (52), and (61) form a set of six conditions for the unknowns $F(r,t)$, $w(t)$, $h_f(t)$ and $b(t)$, the last of which was introduced by extending onto the facet the variable μ. Recalling that four boundary conditions and one initial condition are needed for F owing to the fourth-order PDE (40), we still need one more condition in order to have a reasonably posed free-boundary problem.

We lastly apply continuity of the variable $\mathbf{N}$, the quantity whose divergence yields μ, introduced in Eq. (34). For this purpose we extend $\mathbf{N}$ from the sloping surface outside the facet, $r>w$, where $\mu = (\Omega/a)\nabla\cdot\mathbf{N}$, onto the facet, $r<w$. First, from Eq. (35) and $\mathbf{N} = \hat{\mathbf{e}}_r N(r,t)$ for $r>w$ we have

$$N = ag_1\left(1 + \frac{g_3}{g_1}F^2\right), \quad r > w. \tag{62}$$

Second, we extend $\mathbf{N}$ to the facet region, where $\mathbf{N} = \hat{\mathbf{e}}_r N_f(r,t)$, by

$$\mu_f = \frac{\Omega}{a}\frac{1}{r}\frac{\partial}{\partial r}(rN_f). \tag{63}$$

This equation is readily integrated for N_f by using Eq. (59), where axisymmetry implies that $N_f(0,t)=0$,

$$N_f = ag_1(16B)^{-1}[\dot{h}_f r^3 + 2rb(t)]. \tag{64}$$

The continuity of N across $r=w$, $N(w^+,t)=N_f(w,t)$, thus gives the last condition [recall that $F(w^+,t)=0$],

$$\frac{\dot{h}_f w^3}{16B} + \frac{wb}{8B} = 1. \tag{65}$$

Equations (44), (47), (51), (52), (61), and (65) give the requisite set of seven boundary conditions at the facet edge, $r=w$, and at ∞. Since $b(t)$ is an as yet unknown function, we eliminate it from Eqs. (61) and (65); with $b(t)=8B/w - \dot{h}_f w^2/2B$, the reduced set of conditions at $r=w$ is

$$F = 0,$$

$$1 - \frac{g_3}{g_1} w\,(F^2)_r|_{r=w} = -\frac{\dot{h}_f w^3}{8B},$$

$$1 - \frac{g_3}{g_1} w\,[(F^2)_r + w(F^2)_{rr}]|_{r=w} = -\frac{\dot{h}_f w^3}{2B},$$

$$1 - \frac{g_3}{g_1} w\,[(F^2)_r - 2w(F^2)_{rr} - w^2(F^2)_{rrr}]|_{r=w} = \frac{\dot{h}_f w^3}{B}. \tag{66}$$

By eliminating $\dot{h}_f$ from these equations we obtain the conditions

$$F = 0, \tag{67a}$$

$$\frac{g_3}{g_1} w\,[3(F^2)_r - w^2(F^2)_{rrr}]|_{r=w} = 3, \tag{67b}$$

$$\frac{g_3}{g_1} w\,[3(F^2)_r - w(F^2)_{rr}]|_{r=w} = 3. \tag{67c}$$

Equation (40) is thus solved by imposing the initial condition (43b), along with conditions (52) at $r=\infty$ and (67) at $r=w$. Although we now seem to have a reasonably posed free-boundary problem in the mathematical sense, the issue of the boundary conditions remains a topic of discussion.[31] In particular, our conditions that stem from the continuous extension of the variables μ and **N** onto the facet appear to be consistent with the global variational approach described in Ref. 30; because these authors expand the chemical potential in Fourier series and finally retain a finite number of terms in the expansions, they effectively treat μ as a variable continuous everywhere.

III. BOUNDARY-LAYER THEORY FOR DL KINETICS WITH AXISYMMETRY

As emphasized in Sec. II C, we treat shape evolution as a free-boundary problem where the PDE for the gradient profile, Eq. (40) for DL kinetics and axisymmetric structures, must be supplemented with boundary conditions at the moving boundary of the facet, $r=w(t)$. The formulation of Sec. II is valid for arbitrary positive energies g_1 (line tension) and g_3 (step-step interaction). In particular, we note that only the dimensionless ratio g_3/g_1 enters the PDE, Eq. (40), while the material parameter B simply scales time. Motivated by kinetic simulations [for example, Figs. 4(b) and 6 of Ref. 32], we recognize that for $g_3/g_1 < O(1)$ there exist two distinct regions where the slope profile $F(r,t)$ has different behaviors: an "outer" region, where the slope profile varies relatively slowly in distance and the line-tension energy term proportional to g_1 is important, and an "inner" region adjacent to the edge of the facet, or a boundary layer, where the slope profile varies rapidly from the value $F=0$ at $r=w$ to the values near the boundary with the outer region. In the sense described below, inside the inner region the step-step interaction energy term proportional to g_3 is also significant. Because the simulation results of Ref. 32 correspond to different, small values of a parameter, g, which is proportional to the ratio g_3/g_1 as explained further in Sec. V, we use the parameter

$$\epsilon = \frac{g_3}{g_1}, \tag{68}$$

and further assume that $\epsilon < O(1)$; note that $F=F(r,t;\epsilon)$. Because this ϵ multiplies the spatial derivatives in Eq. (40), including the highest derivative, we can treat the shape evolution described by the boundary-value problem of Sec. II C analytically using boundary-layer theory.[64]

A. Outer solution

We start with the solution of Eq. (40) for $\epsilon=0$ where the corresponding facet radius $w(t;\epsilon)$ is denoted $w(t;0)=w_0(t)$. In this limit only the line tension (g_1 term) determines the shape evolution. From Eq. (40), the resulting zeroth-order solution $F(r,t;0)=F_0(r,t)$ satisfies the PDE $\partial F_0/\partial t = 3B/r^4$, which is trivially integrated subject to the initial condition (43b) to give

$$F_0(r,t) = \frac{3Bt}{r^4} - H'(r), \quad r > w_0(t), \tag{69}$$

and $F_0=0$ for $r<w_0(t)$. The zeroth-order height profile outside the facet is

$$h_0(r,t) = \frac{Bt}{r^3} + H(r), \quad r > w_0(t), \tag{70}$$

and $h_0(r,t)=h_{f0}(t)$ on the facet, for $r<w_0(t)$. At the facet edge, $F_0(w_0,t) = 3Bt/w_0^4 - H'(w_0^+) \neq 0$ because $H'(w_0^+)<0$ by definition of the initial slope; so, the slope profile is discontinuous and condition (67a) is thus not satisfied. This failure of the zeroth-order solution to satisfy a boundary condition at the facet edge motivates the singular perturbation analysis of Sec. III B. In addition, conditions (67b) and (67c) are violated for $\epsilon=0$.

Before we proceed to examine how the inclusion of a nonzero ϵ modifies the slope profile F, we derive a formula

for $w_0(t)$ starting with Eq. (69) and imposing only current and height continuity at the facet edge, $r=w_0(t)$. Although F_0 is not acceptable as a solution of the full boundary-value problem, the zeroth-order facet radius w_0 determined this way is the limit of $w(t;\epsilon)$ as $\epsilon\to 0$ within our continuum approach, as shown in Sec. III B below. The current and height continuity for $\epsilon=0$ give a scaling with time t for $w_0(t)$ that is in agreement with the kinetic simulations for an initial conical profile[32] as we demonstrate below; furthermore, we derive the scaling with time for other initial shapes (see Appendix A). The scaling results are expected to remain valid to leading order in ϵ.

From Eq. (45) with $\epsilon=0$, the surface current outside the facet is $\mathbf{j}_0=j_0(r,t)\hat{\mathbf{e}}_r$ where $j_0(r,t)=(B/\Omega)(1/r^2)$. The current on the facet is given by Eq. (46) with $h_f(t)=h_{f0}(t)$. So, current continuity implies

$$-\dot{h}_{f0}=\frac{2B}{w_0^3}. \tag{71}$$

By virtue of Eq. (70), the height continuity yields

$$h_{f0}=\frac{Bt}{w_0^3}+H(w_0). \tag{72}$$

Combining Eqs. (71) and (72), the facet radius, $w_0(t)$, is thus given implicitly by (see Appendix A for details)

$$w_0(t)\int_W^{w_0(t)} dr r^2[-H'(r)]=3Bt, \quad w_0(0)=W. \tag{73}$$

An explicit relation between $\dot{w}_0$ and w_0 is obtained via differentiation in t of both sides of Eq. (73), or the use of Eq. (A3) of Appendix A:

$$\dot{w}_0=\frac{3B}{w_0^3}\left[\frac{3Bt}{w_0^4}-H'(w_0^+)\right]^{-1}>0. \tag{74}$$

Analytical formulas for $w_0(t)$ for various initial profiles are derived in Appendix A. In particular, Eq. (73) is solved explicitly for an initial conical shape, with slope profile $H'(r)=-\kappa=\text{const}<0$; for sufficiently long times we find [see Eq. (A10) of Appendix A]

$$w_0(t)\sim\left(\frac{9Bt}{\kappa}\right)^{1/4} \quad \text{as } t\to\infty. \tag{75}$$

The $t^{1/4}$ scaling of $w_0(t)$ agrees with that observed for w in kinetic simulations.[32] In general, the scaling behavior of the facet width, $w(t;\epsilon)$, with time is determined by the initial slope profile outside the facet. We next address the scaling of the slope profile $F(r,t;\epsilon)$ with the dimensionless energy parameter $\epsilon=g_3/g_1$.

B. Inner solution

We consider the region adjacent to the edge of the facet, $r=w$, to examine analytically how the inclusion of a nonzero ϵ in the PDE (40) renders the slope F continuous via enforcing the boundary conditions (67). In the spirit of boundary-layer theory,[64] we consider a region of width $\delta=\delta(t;\epsilon)$, $\delta \ll w$, in the neighborhood of the facet edge, where the slope profile varies rapidly, and describe F in this region in terms of the local variable

$$\eta=\frac{r-w(t;\epsilon)}{\delta(t;\epsilon)}. \tag{76}$$

Also, we retain the highest spatial derivative on the right-hand side of Eq. (40) and balance this derivative with the rest of terms in this equation to leading order in ϵ.

The slope profile in the variables η and t is denoted $F=\mathcal{F}(\eta,t;\epsilon)$; $\eta=O(1)$ inside the boundary layer, or the inner region, and $\eta\gg 1$ in the outer region. By direct substitution into Eq. (40), the PDE for $\mathcal{F}$ is

$$\frac{\dot{w}\mathcal{F}_\eta}{\delta}+\left(\eta\frac{\dot{\delta}}{\delta}\mathcal{F}_\eta-\mathcal{F}_t\right)+\frac{3B}{(\eta\delta+w)^4} =\frac{B\epsilon}{\delta^4}\left[(\mathcal{F}^2)_{\eta\eta\eta\eta}+\frac{2\delta}{\eta\delta+w}(\mathcal{F}^2)_{\eta\eta\eta}-\frac{3\delta^2}{(\eta\delta+w)^2}(\mathcal{F}^2)_{\eta\eta} +\frac{3\delta^3}{(\eta\delta+w)^3}(\mathcal{F}^2)_\eta-\frac{3\delta^4}{(\eta\delta+w)^4}\mathcal{F}^2\right], \tag{77}$$

where $\mathcal{F}_\eta=(\partial\mathcal{F}/\partial\eta)$ and $\mathcal{F}_t=(\partial\mathcal{F}/\partial t)$; for $\delta\ll w$ and $\eta=O(1)$, it is advantageous to write Eq. (77) in the form

$$\frac{\dot{w}\delta^3}{B\epsilon}\mathcal{F}_\eta-(\mathcal{F}^2)_{\eta\eta\eta\eta}=O\left(\frac{\delta}{w},\frac{\delta^4}{\epsilon w^4},\frac{\delta^4\mathcal{F}_t}{\epsilon B},\frac{\delta^3\dot{\delta}}{\epsilon B}\right). \tag{78}$$

The PDE (78) is solved inside the boundary layer, where $\eta=O(1)$, via imposing the three conditions (67) at $\eta=0$. One more boundary condition is given by the common limit ("overlap") of the inner and the outer solutions when $\eta\to\infty$ and $r\to w^+$ simultaneously. Specifically, $\mathcal{F}(\eta,t)$ should approach the outer solution, Eq. (69):

$$\mathcal{F}(\eta,t)\sim\frac{3Bt}{w(t)^4}-H'(w(t)^+), \quad \eta\to\infty. \tag{79}$$

We further seek a long-time similarity solution,[65] which depends separately on the local variable η and the time t inside the inner region. To leading order in ϵ, we thus anticipate that

$$\mathcal{F}(\eta,t)\sim a_0(t)f_0(\eta;\epsilon), \tag{80}$$

where, as shown below, f_0 depends implicitly on ϵ via the boundary conditions (67) and $a_0=O(1)$.

1. Scaling of the boundary-layer width

We next derive a scaling of δ with ϵ. Substitution of Eq. (80) into (78) gives

$$\frac{\dot{w}\delta^3}{B\epsilon a_0}f_0'-(f_0^2)''''=O\left(\frac{\delta}{w},\frac{\delta^4}{\epsilon w^4},\frac{\delta^4\dot{a}_0}{\epsilon B},\frac{\delta^3\dot{\delta}}{\epsilon B}\right), \tag{81}$$

where the terms on the right-hand side are shown below to be negligible; see Appendix B for other technical details. By definition of the boundary layer and the variable η, f_0 should satisfy a differential equation in η with coefficients independent of time. From Eq. (81), $\dot{w}\delta^3/B\epsilon a_0$ must be independent of time and ϵ,

$$\frac{\dot{w}\delta^3}{B\epsilon a_0} = k_0 = O(1), \tag{82}$$

where k_0 is a constant; we take $k_0=1$ without affecting observable quantities such as F and w. Thus, to leading order in ϵ,

$$\delta = O(\epsilon^{1/3}), \tag{83}$$

independently of the (axisymmetric) initial conditions. The neglected terms in Eq. (81) are $O(\epsilon^{1/3}) \ll 1$. Then, integrating Eq. (82) for $k_0=1$ yields a formula for $w(t)$ to be used below,

$$w(t) = \left[4B \int_{t_0}^{t} dt' a_0(t') \tilde{w}(t')^3 + w(t_0)^4 \right]^{1/4}, \tag{84}$$

where $\tilde{w} \equiv w/\Delta$, $\Delta(t) \equiv \epsilon^{-1/3}\delta(t;\epsilon) = O(1)$, and t_0 is a fixed yet sufficiently long arbitrary time. The scaling result of Eq. (83) agrees well with kinetic simulations as shown in Sec. V A below.

2. Complete solution for the slope profile

An ODE for $f_0(\eta)$ follows from Eq. (81) with (82). This ODE can be integrated once via applying condition (79) to the similarity form (80). The choice

$$a_0(t) = \frac{3Bt}{w^4} - H'(w^+) \tag{85}$$

determines the explicit time dependence of the slope profile, and yields the conditions

$$\lim_{\eta\to+\infty} f_0(\eta) = 1, \quad \lim_{\eta\to+\infty} f_0'(\eta) = 0. \tag{86}$$

The resulting equation for $f_0(\eta)$ is

$$(f_0^2)''' = f_0 - 1. \tag{87}$$

This equation is universal in the sense that no apparent restriction other than axisymmetry has been imposed for its derivation. In principle, $f_0(\eta)$ can be obtained uniquely via the prescribed conditions (67) and (86). In particular, the conditions at $\eta=0$ are

$$f_0(0) = 0, \tag{88a}$$

$$a_0^2\tilde{w}[3\epsilon^{2/3}(f_0^2)'_{\eta=0} + \tilde{w}^2] = 3, \tag{88b}$$

$$a_0^2\tilde{w}\epsilon^{1/3}[3\epsilon^{1/3}(f_0^2)' - \tilde{w}(f_0^2)'']_{\eta=0} = 3. \tag{88c}$$

In order to solve Eqs. (86)–(88), it is convenient to parametrize f_0 by the independent constants that enter its expansions for small or large η. Specifically, the behavior of $f_0(\eta)$ near the facet edge, $\eta=0$, is obtained from Eq. (87) by taking $(f_0^2)'''+1 \approx 0$,

$$f_0(\eta) \sim c_1\eta^{1/2} + c_3\eta^{3/2}, \quad c_1 > 0, \quad \eta \to 0^+, \tag{89}$$

where c_1 and c_3 are arbitrary. The higher-order terms in this expansion are of the form $c_j\eta^{j/2}$, where $j=5,6,\ldots$; as shown in Appendix C, the coefficients c_j $(j \geqslant 5)$ are known in terms of c_1 and c_3. We thus implicitly parametrize f_0 by c_1 and c_3, use the relations $(f_0^2)'_{\eta=0}=c_1^2$ and $(f_0^2)''_{\eta=0}=4c_1c_3$, and rewrite conditions (88b) and (88c) in terms of c_1 and c_3 as

$$a_0^2\tilde{w}[3\epsilon^{2/3}c_1^2 + \tilde{w}^2] = 3, \tag{90a}$$

$$a_0^2\epsilon^{1/3}\tilde{w}[3\epsilon^{1/3}c_1^2 - 4\tilde{w}c_1c_3] = 3, \tag{90b}$$

where $\tilde{w}$ was defined following Eq. (84).

We note that the square-root (singular) behavior $O(\sqrt{r-w})$ of F described by the leading term in Eq. (89) is consistent with the local equilibrium,[2] where the surface shape is the Legendre transform of the surface free energy, Eq. (32). However, the prefactor here is time dependent as it involves the moving boundary position, $r=w(t)$. The same (square-root) behavior occurs in the one-dimensional case (with one-rectilinear coordinate);[33] this result is expected because inside the boundary layer, sufficiently close to the facet edge, the facet boundary appears locally straight.[66]

The behavior of $f_0(\eta)$ for $\eta \gg 1$ is derived in Appendix D. We find that Eq. (87) may admit a growing mode in η, which must be suppressed in order that f_0 satisfies the far-field conditions (86). The elimination of this mode [e.g., taking $C=0$ in Eq. (D3) of Appendix D] amounts to imposing a relation between the c_1 and c_3 of Eq. (89).

We solve the ODE (87) numerically applying conditions (86) and (88a). For this purpose, we fix c_1 and integrate the ODE starting from $\eta_0 \ll 1$, where values of $f_0(\eta)$ and its derivatives are evaluated by using expansion (C1) of Appendix C, towards $\eta^* \gg 1$ to satisfy the condition $f_0(\eta^*) \approx 1$. So, we find a family of similarity solutions $f_0(\eta)$, parametrized by c_1, which correspond to a curve $c_3(c_1)$ where $c_3 < 0$. Representative numerical solutions are shown in Fig. 2(a). The solution $f_0(\eta)$ and the facet radius $w(t)$ are obtained uniquely via imposing the remaining conditions at $\eta=0$, Eqs. (90), along with Eq. (84). Below we illustrate this procedure and show how the unique similarity shape $f_0(\eta)$ and facet radius $w(t)$ depend on ϵ for the case with a conical initial shape.

Once $f_0(\eta)$ and $w(t)$ are known, the slope profile everywhere outside the facet is obtained by adding the outer and inner solutions and subtracting their overlap. The resulting composite formula reads

$$F(r,t) \sim \left[\frac{3Bt}{w^4} - H'(w^+) \right][f_0(\eta) - 1] + \frac{3Bt}{r^4} - H'(r). \tag{91}$$

3. Conical initial shape

The formulation described above applies to a class of axisymmetric initial shapes. We next restrict our analysis to the case with a conical initial shape of unity slope outside the facet, $H'(r)=-1$ for $r>W$, determine uniquely the solution $f_0(\eta)$, and discuss the scaling of this solution with ϵ. The boundary-value problem of Eqs. (86), (87), and (88a) and (90) can be solved via the observation that Eq. (84) for the facet radius is consistent with formulas (85) for $a_0(t)$ and

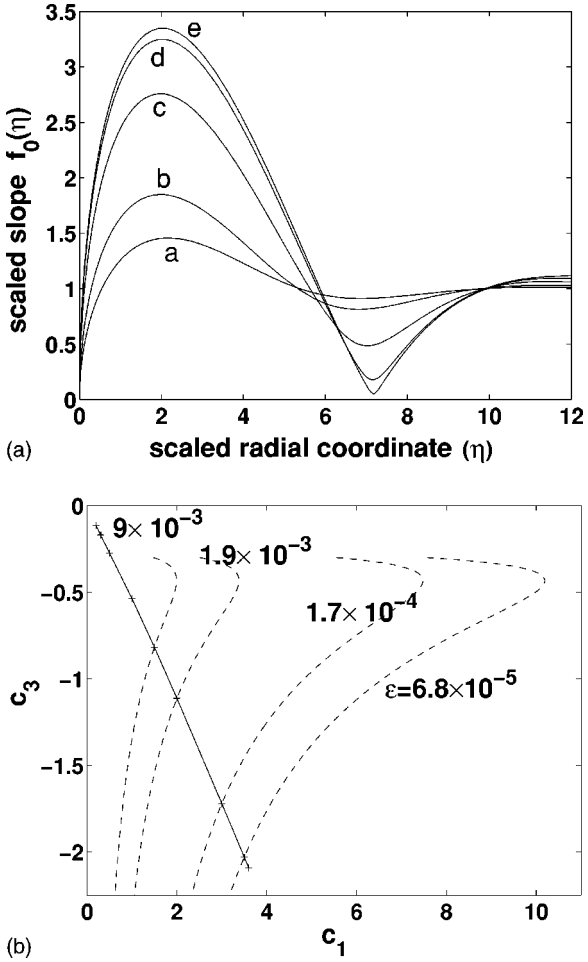

FIG. 2. (a) Numerical solutions of Eq. (87) with the boundary conditions $f_0(0)=0$ and $f_0(\infty)=1$. Curves a–e are parametrized by $(c_1,c_3)=(1.5,-818\,354\,8)$, $(2,-1.113\,031)$, $(3,-1.721\,075\,02)$, $(3.5,-2.030\,210\,2)$, $(3.6,-2.092\,321\,55)$ and correspond to $\epsilon=9.2\times10^{-3}$, 1.9×10^{-3}, 1.7×10^{-4}, 6.8×10^{-5}, 5.7×10^{-5}. (b) The dashed curves are described by Eq. (101) for a conical initial shape and different ϵ, while the solid curve shows c_3 as a function of c_1 from the numerical solutions of Eq. (87) in part (a).

(75) for $w(t;0)$ if $\tilde{w}$ and a_0 are constants for long times; so, the boundary-layer width, $\delta(t)$, increases with time at the same rate as the facet radius, $w(t)$.

It turns out that significant analytical progress is possible in this case, though at the expense of some algebra. To arrive at the analytical results it is convenient to define the parameters $\tilde{c}_1$ and λ by

$$c_1=(\tilde{c}_1\epsilon^{-1/3})\tilde{w}, \tag{92a}$$

$$\tilde{w}^3a_0^2\lambda^2=3, \tag{92b}$$

where $\lambda>0$ for definiteness. Our purpose is to use λ as a free parameter in order to relate c_3, c_1 and ϵ. By virtue of definitions (92), conditions (90) become

$$3\tilde{c}_1^2+1=\lambda^2, \quad 3\tilde{c}_1^2-4\tilde{c}_1c_3=\lambda^2. \tag{93}$$

Hence, $\lambda>1$ and $4\tilde{c}_1c_3=-1$, by which

$$\tilde{c}_1=3^{-1/2}\sqrt{\lambda^2-1}, \quad c_3=-4^{-1}\sqrt{3}(\lambda^2-1)^{-1/2}; \tag{94}$$

note that $c_3<0$ consistently with the numerical solution of Fig. 2(a). Because the parameters $\tilde{w}$, a_0, c_1 and c_3 depend on ϵ, λ is an implicit function of ϵ; in the limit $\epsilon\to0^+$, λ approaches 1 from higher values ($\lambda\to1^+$).

We proceed to express a_0 and $\tilde{w}$ in terms of λ. For long times t, Eq. (84) reduces to

$$w(t)\sim(4Ba_0\tilde{w}^3t)^{1/4}. \tag{95}$$

The combination of this formula with Eq. (85) for $H'(w^+)=-1$ gives a quadratic equation for a_0 which has the admissible (positive) solution

$$a_0=\frac{1}{2}+\frac{1}{2}\sqrt{1+\frac{3}{\tilde{w}^3}}. \tag{96}$$

Substitution of this formula into Eq. (92b) gives

$$\tilde{w}=\left[\frac{3}{16}\frac{(4-\lambda^2)^2}{\lambda^2}\right]^{1/3}. \tag{97}$$

By using Eq. (96) the amplitude a_0 is thus calculated as a function of λ,

$$a_0=\frac{1}{2}+\frac{1}{2}\sqrt{1+\frac{16\lambda^2}{(4-\lambda^2)^2}}=\frac{|4-\lambda^2|+(4+\lambda^2)}{2|4-\lambda^2|}. \tag{98}$$

The combination of Eqs. (95), (97), and (98) gives

$$\frac{w(t;\epsilon)}{(Bt)^{1/4}}\sim\left\{\frac{3}{8}\frac{[|4-\lambda^2|+(4+\lambda^2)]|4-\lambda^2|}{\lambda^2}\right\}^{1/4}, \tag{99}$$

which provides an explicit analytical solution for the facet width, w, as a function of ϵ once λ is determined as a function of ϵ; see Eqs. (100) below. Note that in the limit $\epsilon\to0^+$, or $\lambda\to1^+$, formula (99) reduces to $w(t;0)\sim(9Bt)^{1/4}$, in agreement with expression (75) for $\kappa=1$.

It remains to express in terms of λ the coefficients c_1 and c_3 introduced in Eq. (89) and thereby determine analytically the ϵ-dependent curves $c_3(c_1;\epsilon)$. From Eqs. (92a), (94), and (97),

$$c_1=\epsilon^{-1/3}3^{-1/2}\left[\frac{3}{16}\frac{(4-\lambda^2)^2}{\lambda^2}\right]^{1/3}\sqrt{\lambda^2-1}, \tag{100a}$$

$$c_3=-\frac{\sqrt{3}}{4}(\lambda^2-1)^{-1/2}. \tag{100b}$$

For each value of ϵ, these equations describe implicitly a relation between c_1 and c_3 in terms of the (free) parameter λ. By eliminating λ from Eqs. (100) we find

$$c_1\epsilon^{1/3}=-\frac{3}{4c_3}\left[\frac{1}{16^2c_3^2}\frac{(16c_3^2-1)^2}{16c_3^2+3}\right]^{1/3}, \quad c_3<0. \tag{101}$$

This equation describes a one-parameter family of curves, each curve corresponding to a different value of ϵ. Representative members of this family for four different values of (small) ϵ are shown in Fig. 2(b).

The intersection of the curve of Eq. (101) with the set of points (c_1,c_3) that result from solving numerically Eqs. (86),

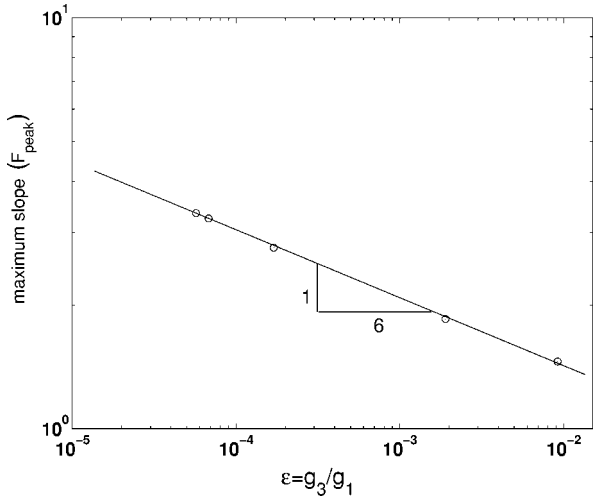

FIG. 3. Log-log plot of the maximum of $f_0(\eta;\epsilon)$, $(f_0)_{\max}$, as function of ϵ from the solution of Eq. (87) with conditions $f_0(0)=0$ and $f_0(\infty)=1$ and Eq. (101). The circles represent the results of our numerical calculations and correspond to the solution curves a–e of Fig. 2(a). The straight line describes the $\epsilon^{-1/6}$ scaling law derived analytically, Eq. (103).

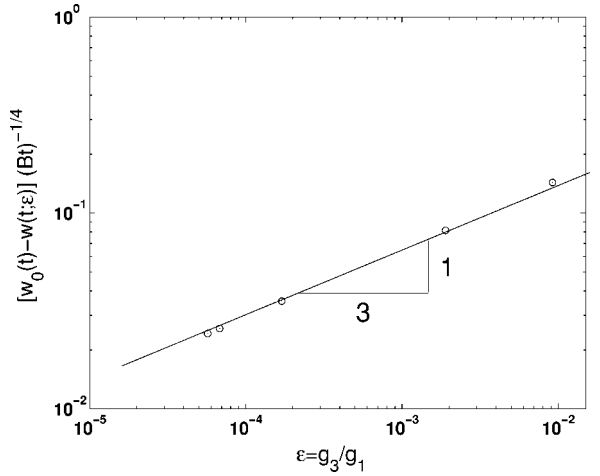

FIG. 4. Log-log plot of the difference $[w_0(t)-w(t;\epsilon)](Bt)^{-1/4}$ as function of ϵ from the solution of Eq. (87), with conditions $f_0(0)=0$ and $f_0(\infty)=1$, and Eqs. (99), (100b), and (101). The circles represent the results of our numerical calculations and correspond to the solution curves a–e of Fig. 2(a). The straight line describes the $\epsilon^{1/3}$ scaling law of Eq. (104).

(87), and (88a) is shown in Fig. 2(b), and determines a single value of ϵ for each of the solution curves of Fig. 2(a). Conversely, to each value of ϵ there corresponds a unique pair (c_1,c_3), which comes from the intersection of two curves in Fig. 2(b), and hence a unique solution $f_0(\eta;\epsilon)$; as ϵ decreases, c_1 and $|c_3|$ increase. Note that, by using the full set of our proposed boundary conditions, we have arrived at a unique solution for the slope profile as a function of time t and distance r, and hence resolved the uniqueness problem first noted by Israeli and Kandel.[32]

There is one more scaling law that stems from the analysis. Each of the solution curves $f_0(\eta)$ has a well-defined absolute maximum located at $\eta=\eta_{\rm m}$. An order-of-magnitude estimate of this maximum is obtained by differentiation of formula (89),

$$(f_0)_{\max}=f_0(\eta_{\rm m})\sim\frac{2c_1}{3}\sqrt{\frac{c_1}{3|c_3|}}, \tag{102a}$$

$$\eta_{\rm m}\sim\frac{c_1}{3|c_3|}. \tag{102b}$$

Because the local-coordinate description describes the shape as independent of ϵ, the position of this maximum, $\eta_{\rm m}$, should be independent of ϵ to leading order. Thus, according to Eq. (102b), $c_1=O(|c_3|)$; the same conclusion is reached by inspection of the numerical curve in Fig. 2(b). Equation (101) then dictates that c_1 and c_3 are $O(\epsilon^{-1/6})$ and so the maximum slope, $(f_0)_{\max}$, is estimated by Eq. (102a) to be $O(\epsilon^{-1/6})$,

$$(f_0)_{\max}=O(\epsilon^{-1/6}). \tag{103}$$

In Fig. 3 we plot the numerically evaluated maximum of f_0 corresponding to the solution curves a–e of Fig. 2(a) versus ϵ, and verify the $\epsilon^{-1/6}$ scaling law. This scaling result is also in excellent agreement with kinetic simulations[32] as demonstrated in Sec. V A below.

Once (c_1,c_3) are determined for each ϵ, the parameter λ is found as a function of ϵ by use of Eqs. (100). Thus, a_0 and w are determined as functions of ϵ via Eqs. (98) and (99); in the limit $\epsilon\to 0$, a_0 and w are $O(1)$ as expected. In particular, as ϵ decreases towards 0, $w/(Bt)^{1/4}$ behaves as $w/(Bt)^{1/4}\sim[3(4/\lambda^2-1)]^{1/4}$, and thus increases to the value $w_0(t)/(Bt)^{1/4}=\sqrt{3}$, where $w_0(t)=w(t;0)$. Hence, for $c_1=O(|c_3|)$ from Eq. (102b) or Fig. 2(b) and by use of Eq. (100b), we obtain the variation of the facet width with ϵ,

$$w(t;0)-w(t;\epsilon)=O(\epsilon^{1/3})>0. \tag{104}$$

In Fig. 4 we plot the difference $[w_0(t)-w(t;\epsilon)](Bt)^{-1/4}$ corresponding to the solution curves a–e of Fig. 2(a) versus ϵ, and verify our analytically predicted $\epsilon^{1/3}$ scaling law. In addition, the monotonically decreasing and scaling behavior of $w/(Bt)^{1/4}$ with ϵ predicted here analytically agrees with kinetic simulations[32] as shown in Sec. V A below.

IV. BOUNDARY-LAYER THEORY FOR ADL KINETICS WITH AXISYMMETRY

We next address the scaling of the boundary-layer width with $\epsilon=g_3/g_1$ for ADL kinetics, where ϵ is the ratio of step-step interaction energy to line tension. Physically, in this case the attachment and detachment of atoms to and from the step edges is the rate-limiting process in the surface relaxation. From the mathematical standpoint, the continuum equations may be more difficult to study. For example, the effective surface diffusivity in the governing equation (27) is $\mathcal{D}_{\rm s}=D_{\rm s}(1+mF)^{-1}\sim D_{\rm s}m^{-1}F^{-1}$, and thus appears to become singular when $F\to 0$;[67] see Eq. (22). In ADL kinetics the behavior of the step configuration is more complicated; a wealth of physical phenomena and mathematical features exclusive to

this limit arise which, within the continuum approach and boundary-layer ideas, require considerations different from those of Sec. III.

Despite the additional complications, however, kinetic simulations[32] indicate to us that the continuum step density, $F(r,t)$, in ADL kinetics retains a feature common with DL kinetics: F still varies rapidly close to the facet, inside a boundary layer (inner region) whose width depends nontrivially on the ratio g_3/g_1 [e.g., see Figs. 5(b), 5(d) and 7 of Ref. 32]. Before we focus on this continuum aspect, we describe the main physical features of ADL kinetics that emerge from kinetic simulations, and discuss their implications for the application of boundary-layer theory.

A. Implications of kinetic simulations

The results of kinetic simulations[32,41] for ADL kinetics indicate that the behavior of the step positions $r_i(t)$, which satisfy Eqs. (6)–(10) and the initial condition of given $r_i(0)$, can be radically different from that for DL kinetics. Specifically, there are two interrelated features of step motion in ADL kinetics that characterize such differences: (a) For fixed and not too small ratio of step-step interaction energy to line tension, the motion of several steps adjacent to the first step undergoes abrupt changes as the top layer shrinks and is about to collapse; thus, this motion is sensitive to the details of kinetics energetics of the top layer. In contrast, in DL kinetics the motion of steps appears to be uniform along the distance from the first step (see Fig. 2 of Ref. 32). (b) When the ratio of repulsive step interaction energy to line tension decreases below a threshold value, the step configuration becomes unstable as the steps start to form a bunch close to the facet; further reduction of the ratio of the two energies causes the appearance of more bunches and the notion of evolution as driven by individual steps becomes questionable [see Figs. 5(a), 5(c), 5(e) and 5(f) of Ref. 32]. In DL kinetics, on the other hand, no such instability occurs; the decrease of the ratio of the two energies, g_3/g_1, simply causes a rise of the (discrete) step density, $F_i=a/(r_{i+1}-r_i)$, close to the facet [see Fig. 4(a) of Ref. 32]. In view of these complications, the issue is raised whether a similarity solution for the continuum step density is valid close to the facet and, if so, what is its form. Another, fundamental issue is the validity of the continuum theory for ADL kinetics, and the incorporation in a continuum model of the motion of the top step(s) in the form of suitable boundary conditions.

In particular, because of feature (a) above, F should change within the collapse period of the top step; a similarity solution of form (80) then seems inconsistent with such changes because it cannot account for the details of motion of the top step. In fact, Eq. (80) is expected to be valid only sufficiently far from the facet,[68] where the local, inner variable, η, exceeds some value. For lower values of η, the maximum of the similarity function appears sensitive to the density of the first few steps for pure ADL kinetics.[68] From the mathematical standpoint, as explained in Ref. 41, the step density very near the facet has a strong temporal, almost-periodic behavior related to the motion of the top step.

In addition, feature (b) above, which refers to the step bunching instability for ADL kinetics, gives rise to an issue more serious for the continuum approach as not only is self-similarity of the shape then lost, but also the continuum approximations that give the governing equation (27) seem to break down because F can vary over lengths comparable to a terrace width; in ADL kinetics the continuum limit has to be reconsidered when g_3/g_1 becomes sufficiently small.[69] Hence, taking $\epsilon=g_3/g_1=0$ for ADL kinetics within boundary-layer theory[64] in order to determine the form of the outer solution is apparently forbidden by the conditions of validity of the continuum theory. Nevertheless, we show that our continuum predictions provide quantitative insight into certain aspects of ADL kinetics.

Because of the potential complications discussed in the preceding paragraphs, our focus here is on the scaling of the boundary-layer width. We circumvent the difficulties outlined above by making the following assumptions in the case with ADL kinetics: (a) We allow for a long-time similarity solution that, though still dependent on a local coordinate, η, in the inner region, also has an explicit time dependence related to the periodic motion of the top step; we subsequently argue that this latter dependence can be neglected for our scaling purposes. (b) Because the outer solution, which is usually defined through taking $\epsilon=0$ in the governing equation, is ill-defined, we do not address the issue of finding a unique slope profile. Instead, we assume that ϵ exceeds the critical value below which the bunching instability occurs, and derive a scaling of the boundary-layer width via balancing terms to leading order in ϵ in the governing equation, in complete analogy with the DL case. In Sec. V B below we show that our scaling predictions are in excellent agreement with the results of kinetic simulations.

The governing PDE for the slope profile, $F(r,t)$, for ADL kinetics results from Eq. (27) by neglecting unity compared to mF, as implied by Eq. (22); so we study the PDE

$$\frac{1}{\breve{B}}\frac{\partial F}{\partial t}=\frac{\partial}{\partial r}\frac{1}{r}\frac{\partial}{\partial r}\frac{1}{r}\left(\frac{1}{F}\right)-\frac{g_3}{g_1}\frac{\partial}{\partial r}\frac{1}{r}\frac{\partial}{\partial r}\left[\frac{r}{F}\frac{\partial}{\partial r}\frac{1}{r}\frac{\partial}{\partial r}(rF^2)\right], \tag{105}$$

where the material parameter $\breve{B}$ is

$$\breve{B}=\frac{c_s(ka)g_1\Omega^2}{2k_BT}. \tag{106}$$

B. Scaling of boundary-layer width

Following the discussion of the preceding section and by analogy with our approach to DL kinetics, we start with the long-time similarity ansatz

$$F(r,t)\sim a_0(t)f_0(\eta,\tau),\quad \eta=\frac{r-w(t;\epsilon)}{\delta(t;\epsilon)}, \tag{107}$$

where $\tau=\tau(t)$ accounts for the motion of the top step; f_0 is in principle a periodic function of τ and varies slowly with t except possibly at times when the top step collapses. Differentiation of Eq. (107) with respect to time t gives

$$\frac{\partial F}{\partial t} = \dot{a}_0 f_0 - a_0 \left[\frac{\partial f_0}{\partial \eta}\left(\frac{\dot{\delta}}{\delta}\eta + \frac{\dot{w}}{\delta} \right) - \frac{\partial f_0}{\partial \tau}\dot{\tau} \right]. \qquad (108)$$

Recall that $\delta \ll w$ for the boundary-layer ideas to be applicable; inside the boundary layer $\eta = O(1)$. We thus take $|(f_0)_\tau \dot{\tau}| \ll |(f_0)_\eta [(\dot{\delta}/\delta)\eta + (\dot{w}/\delta)]|$, which neglects the τ-dependence, and Eq. (108) reduces to

$$\frac{\partial F}{\partial t} \approx \dot{a}_0 f_0 - a_0 \frac{\partial f_0}{\partial \eta}\left(\frac{\dot{\delta}}{\delta}\eta + \frac{\dot{w}}{\delta} \right). \qquad (109)$$

Substitution of Eq. (107) into (105) and use of Eq. (109) gives

$$\frac{1}{\breve{B}}\left[\dot{a}_0 f_0 - a_0 \left(\frac{\dot{\delta}}{\delta}\eta + \frac{\dot{w}}{\delta} \right) \frac{\partial f_0}{\partial \eta} \right]$$
$$= \frac{1}{a_0 \delta^2} \frac{\partial}{\partial \eta} \frac{1}{\eta\delta + w} \frac{\partial}{\partial \eta} \frac{1}{\eta\delta + w} \frac{1}{f_0} - \frac{\epsilon a_0}{\delta^2} \frac{\partial}{\partial \eta} \frac{1}{\eta\delta + w} \frac{\partial}{\partial \eta}$$
$$\times \left\{ \frac{1}{f_0}\left[\frac{\eta\delta + w}{\delta^2} \frac{\partial^2 f_0^2}{\partial \eta^2} + \frac{1}{\delta} \frac{\partial f_0^2}{\partial \eta} - \frac{f_0^2}{\eta\delta + w} \right] \right\}. \qquad (110)$$

The boundary layer is identified with the region where $\eta = O(1)$. For $\epsilon < O(1)$ and $\delta \ll w$, the balance of the leading-order terms in ϵ thus gives

$$\frac{\dot{w}\delta^3}{\breve{B}\epsilon} \frac{\partial f_0}{\partial \eta} - \frac{\partial^2}{\partial \eta^2}\left(\frac{1}{f_0} \frac{\partial^2 f_0^2}{\partial \eta^2} \right) + \frac{\delta^2}{a_0^2 \epsilon w^2} \frac{\partial^2}{\partial \eta^2}\left(\frac{1}{f_0} \right)$$
$$= O\left(\frac{\dot{a}_0 \delta^4}{\breve{B}\epsilon a_0}, \frac{\dot{\delta}\delta^3}{\breve{B}\epsilon}, \frac{\delta}{w} \right), \qquad (111)$$

where we keep only the highest derivatives in the terms pertaining to the two energetic contributions of line tension (g_1 term) and step-step interactions (g_3 term). A distinct difference of Eq. (111) here from the corresponding Eq. (81) for DL kinetics is the presence of the additional derivative $(1/f_0)_{\eta\eta}$ on the left-hand side, which arises from the line-tension term because of the F-dependent effective surface diffusivity.

By inspection of Eq. (111) the only possible balance, which does not lead to inconsistencies, involves all three terms on the left-hand side. Thus, we require that

$$\frac{\dot{w}\delta^3}{\breve{B}\epsilon} = k_0(\tau) = O(1), \qquad (112a)$$

$$\frac{\delta^2}{a_0^2 \epsilon w^2} = k_1(\tau) = O(1), \qquad (112b)$$

where k_0 and k_1 are slowly varying functions of time. Combining these two results we find

$$\delta = O(\epsilon^{3/8}), \qquad (113)$$

which is a prediction of a scaling law for the boundary-layer width under ADL kinetics. This result should be contrasted with the case of DL kinetics where $\delta = O(\epsilon^{1/3})$. The scaling of Eq. (113) is in excellent agreement with kinetic simulations[32] as shown in Sec. V B below. The same argument seems to imply that $w = O(\epsilon^{-1/8})$. However, we have insufficient data to test this idea as the exponent is small and there is difficulty in defining $w(t)$ in the simulations.

V. COMPARISON WITH SIMULATION RESULTS

We next compare the predictions of our continuum approach for DL and ADL kinetics with the kinetic simulations reported by Israeli and Kandel.[32] We believe that this comparison is meaningful as these authors used the potential of Eq. (8) to describe repulsive step interactions between steps of the same sign, and did not include the self-interaction of the top step in their formulation, in analogy with our formulation of Secs. II A and II B. Our approach is based on the PDE (27) for axisymmetric structures whereas the kinetic simulations of Ref. 32 are based on numerical solutions for long times of the kinetic differential equations given in Sec. II A.[70] We exercise some caution in comparing results from these two approaches, however, as the dimensionless parameters used are different.

In particular, in their simulations both for DL and ADL kinetics the authors in Ref. 32 vary a dimensionless parameter, g, proportional to our $\epsilon = g_3/g_1$, $g = (2/3)\mathcal{C}^2 \cdot (g_3/g_1)$, holding g_1 fixed, which in our analysis amounts to changing only ϵ; $\mathcal{C} = k_B T/(\Omega g_1/a)$ is a constant independent of g_3. Their simulations produced a g-dependent family of solutions; see their Figs. 4(b) and 6 for DL kinetics, and their Figs. 5(b), 5(d) and 7 for ADL kinetics. Israeli and Kandel[32] also derived a g-dependent ODE in the similarity variable $x = \mathcal{C}^{1/4} \cdot r/(Bt)^{1/4}$ (not to be confused with the Cartesian coordinate) for the step density $F(r,t)$; we recognize that, for sufficiently small g, their ODE reduces to our Eq. (87). However, on the basis of their equation they found multiple solutions because their analysis lacked one boundary condition at the facet edge, $r = w$. We provide a unique solution $f_0(\eta;\epsilon)$ for each ϵ in the case with DL kinetics, but are unable to treat ADL kinetics on the same detailed footing, as explained in Sec. IV.

A. DL kinetics

We have predicted three scaling laws with $\epsilon = g_3/g_1$ according to the analysis of Sec. III for DL kinetics: (a) The boundary-layer width $\delta(t;\epsilon)$ scales as $\epsilon^{1/3}$, Eq. (83). (b) The maximum step density close to the facet scales as $\epsilon^{-1/6}$, Eq. (103). (c) The facet radius, $w(t;\epsilon)$, is monotonically decreasing in ϵ, and its (positive) change from the limit $w(t;0) = \sqrt{3}(Bt)^{1/4}$, $w(t;0) - w(t;\epsilon)$, scales as $\epsilon^{1/3}$, Eq. (104).

First, we address the scaling of the boundary layer width. In order to compare our results with the kinetic simulations, we define the boundary-layer thickness as the distance from the facet edge, $x_0 = \mathcal{C}^{1/4} \cdot w_0/(Bt)^{1/4}$, to the position, $x_{\text{peak}} = \mathcal{C}^{1/4} \cdot r_{\text{peak}}/(Bt)^{1/4}$, of the peak of the step density, $F_{\text{peak}} = F(r_{\text{peak}}, t)$. In Fig. 5 we show the results of kinetic simulations for the scaled distance $x_{\text{peak}} - x_0$ versus the parameter $g = (\frac{2}{3})\mathcal{C}^2 \cdot \epsilon$, and compare with our $\epsilon^{1/3} \propto g^{1/3}$ prediction. We find the agreement to be very good for a wide range of values of g. A few remarks are in order on the deviations of the

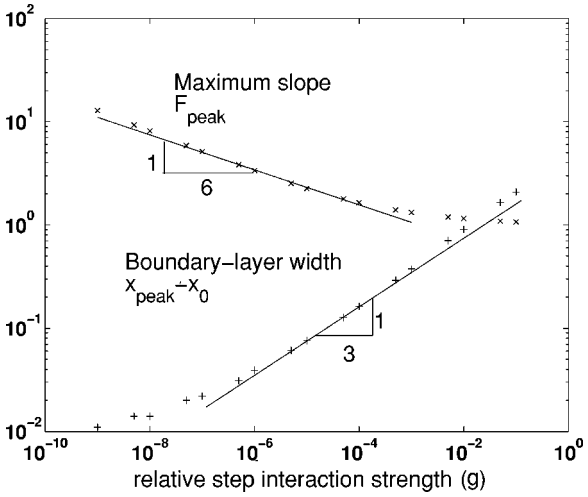

FIG. 5. Log-log plot of the boundary-layer thickness $\delta(t;\epsilon)$ and the maximum of step density F_{peak} as functions of $g=(2/3)\mathcal{C}^2\cdot\epsilon$ for DL kinetics; $\mathcal{C}=k_BT/(\Omega g_1/a)$ is a constant independent of g_3. The crosses represent the results of kinetic simulations given to us by Israeli and Kandel.[32] Here, $\delta(t;\epsilon)$ is estimated as the scaled distance $x_{\text{peak}}-x_0$ between the facet edge, $x_0=\mathcal{C}^{1/4}\cdot w\cdot(Bt)^{-1/4}$, where $F=0$, and the position x_{peak} of the maximum of F. The straight (solid) lines correspond to the $\epsilon^{1/3}$ and $\epsilon^{-1/6}$ scaling laws predicted according to Eq. (81).

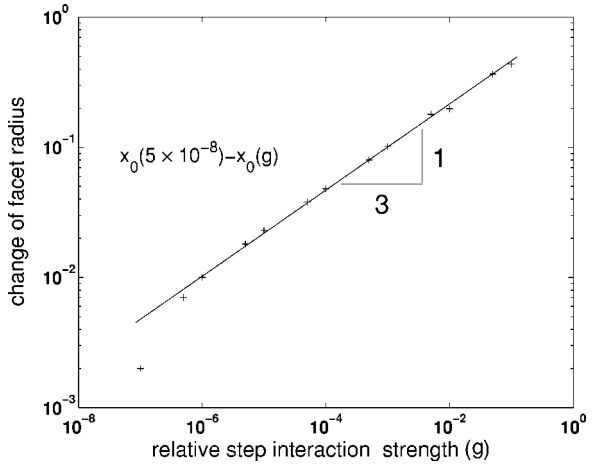

FIG. 6. Log-log plot of the positive, scaled by $(Bt)^{1/4}$, change of the facet radius w from its limiting value as $\epsilon\to 0$, $[w(t;0)-w(t;\epsilon)](Bt)^{-1/4}$, as function of $g=(2/3)\mathcal{C}^2\epsilon$for DL kinetics; $\mathcal{C}=k_BT/(\Omega g_1/a)$ is a constant independent of g_3. The crosses represent the results of kinetic simulations for the change $x_0(5\times10^{-8})-x_0(g)$ given to us by Israeli and Kandel;[32] $x_0(g)=\mathcal{C}^{1/4}\cdot w\cdot(Bt)^{-1/4}$ is the scaled facet radius from kinetic simulations as function of g. The straight (solid) line corresponds to the $\epsilon^{1/3}$ scaling law predicted according to Eq. (99).

boundary-layer width from the predicted behavior when $g<10^{-6}$. As g (or ϵ) decreases towards small values in the simulations, x_{peak} approaches the facet edge, the boundary-layer width becomes small on the scale of the step spacing, and its evaluation in the discrete simulations becomes prone to errors; therefore, the definition of the boundary-layer width as $x_{\text{peak}}-x_0$ is questionable when g is too small.

Next, we examine how the F_{peak} furnished by kinetic simulations varies with g. In Fig. 5 we compare the results of kinetic simulations with the $\epsilon^{-1/6}\propto g^{-1/6}$ scaling prediction. Again, the agreement is very good for an appreciable range of values of g. We note from Fig. 5 that the behavior of F_{peak} starts to deviate from the $g^{-1/6}$ scaling law as g increases to values $O(1)$, because the slope profile near the facet then has relatively slow variations in distance and F_{peak} approaches the constant slope of the conical initial shape, which is unity in the simulations [e.g., see the slope profiles in Fig. 2(a)].

Finally, we examine the predicted sign and scaling with ϵ of the change of the facet radius w from its limit w_0, $w(t;\epsilon)-w(t;0)$. The kinetic simulations furnish the scaled facet radius, $x_0=\mathcal{C}^{1/4}\cdot w/(Bt)^{1/4}$, i.e., the distance where the step density F practically vanishes, to be decreasing in g, in agreement with our prediction, Eq. (99); see Figs. 4(b) and 6 of Ref. 32. In Fig. 6 we plot the positive change of x_0 as a function of g with reference to the value of x_0 at extremely small g, here $g=5\times10^{-8}$. The simulation results are in excellent agreement with our prediction of the $\epsilon^{1/3}$ scaling law. Note that we choose the x_0 evaluated at $g=5\times10^{-8}$ as a reference value recognizing that the facet radius calculated for smaller g by the kinetic simulations is prone to numerical errors as explained above. [We find that the use of kinetic simulation data for x_0 that corresponds to $g\leqslant10^{-8}$ seems to destroy the scaling predicted by Eq. (104).]

B. ADL kinetics

We now turn our attention to the ADL kinetics analyzed in Sec. IV. There is one scaling law that comes from the analysis and can be compared with kinetic simulation data: the boundary-layer width scales as $\epsilon^{3/8}$, Eq. (113).

In this case the solution found by kinetic simulations has a relatively strong temporal behavior related to the periodic motion of the top step, and thus does not have a unique similarity form at distances sufficiently close to the moving facet.[68] Consequently, the position of the maximum of F cannot be used in the definition of the boundary-layer width, $\delta(t;\epsilon)$. Because F attains a unique similarity form at distances $x\geqslant x_{\min}$, where $x=\mathcal{C}^{1/4}\cdot r\cdot(Bt)^{-1/4}$ and $x_{\min}$ corresponds to the position of the first (nonzero) minimum of F closest to the facet, we define $\delta(t;\epsilon)$ as the difference $x_{\min}-x_0$ between the facet edge, $x_0=\mathcal{C}^{1/4}\cdot w\cdot(Bt)^{-1/4}$, and $x_{\min}$.

In Fig. 7 we show the results of kinetic simulations for the scaled distance $x_{\min}-x_0$ versus $g=(2/3)\mathcal{C}^2\cdot\epsilon$, and compare with our $\epsilon^{3/8}$ prediction. We find the agreement to be excellent for a wide range of values of g, $5\times10^{-4}<g\leqslant1$; note that smaller values of g have been shown[32] to drive the system to a step bunching instability and may thus be irrelevant to the similarity solutions under consideration.

VI. SUMMARY AND DISCUSSION

By using a continuum description based on thermodynamic principles and mass conservation we studied aspects of morphological relaxation of single-faceted crystal surfaces below the roughening transition temperature with focus on axisymmetric surface profiles. Our approach is a blend of three elements. The first element is a PDE for the surface height profile h, Eq. (37), which reduces to Eq. (29) for

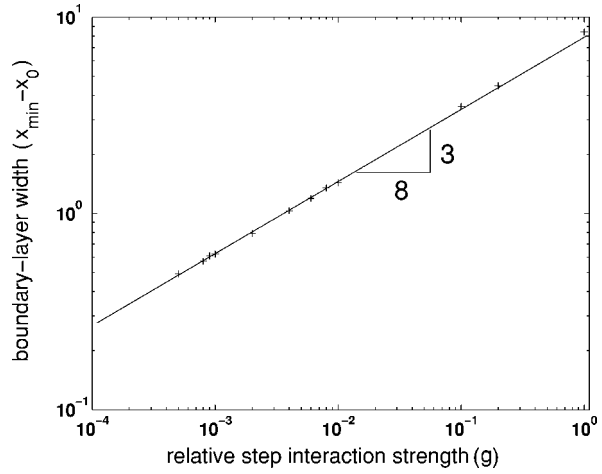

FIG. 7. Log-log plot of the boundary-layer thickness $\delta(t;\epsilon)$ as function of $g=(2/3)C^2\cdot\epsilon$ for ADL kinetics; $C=k_BT/(\Omega g_1/a)$ is a constant independent of g_3. The crosses represent the results of kinetic simulations given to us by Israeli and Kandel.[32] Here, $\delta(t;\epsilon)$ is estimated as the scaled distance $x_{min}-x_0$ between the facet edge, $x_0=C^{1/4}\cdot w\cdot(Bt)^{-1/4}$, and the position x_{min} of the minimum of F, where the similarity solution is well-defined. The straight (solid) lines correspond to the $\epsilon^{3/8}$ scaling law predicted according to Eq. (113).

axisymmetric shapes. Equation (27) was derived from the kinetic equations of a step-flow model, Eqs. (6)–(10), or, alternatively, from a coarse-grained surface free energy approximated by Eq. (32) for simple, repulsive pairwise step interactions. This PDE accounts for the main step energetics, namely, line-tension energy and step-step interaction energy. The second ingredient of our approach is free-boundary theory to treat the expanding facet in the spirit of Spohn;[23] we extended the analysis further, to cases where both the line tension and the step interactions play an important role. The third element is singular perturbation theory, particularly boundary-layer theory, by which we described systematically rapid variations of self-similar slope profiles F close to the facet.

The combination of free-boundary and boundary-layer theories for DL kinetics enabled us to make two analytical advances over past continuum treatments. (a) We were able to simplify the PDE for the slope profile close to the facet by reducing it a universal ODE, Eq. (87), for some class of axisymmetric shapes. Furthermore, by exploiting the hierarchy of the continuum equations, as expressed by the relations among the surface free energy per projected area, the chemical potential, the surface current and the height time derivative, Eqs. (1), (30), (33), and (34), we identified a set of boundary conditions for F at the facet edge that provided us with a unique solution to the ODE for each value of g_3/g_1. (b) We found scaling laws for the boundary-layer width, the maximum slope and the facet radius as functions of the ratio of step interactions to line tension that agree well with kinetic simulations. Specifically, the boundary-layer width scales as $(g_3/g_1)^{1/3}$, the maximum slope scales as $(g_3/g_1)^{-1/6}$, and the change of the facet radius from its limiting value (as $g_3/g_1\to 0$) scales as $(g_3/g_1)^{1/3}$.

For ADL kinetics we have recognized difficulties in applying boundary-layer theory because of the instabilities that arise in the step motion when $\epsilon=g_3/g_1$ is sufficiently small. One difficulty is finding a suitable ansatz for the outer solution, which usually results from taking $\epsilon=0$ in the equation of motion. In this case, the difficulty is related to the strong dependence of the slope profile close to the facet on the motion of the top step. Despite these features we have been able to identify a boundary layer for the slope profile close to the facet and quantify its dependence on the step energetics: the boundary-layer width scales as $(g_3/g_1)^{3/8}$; this scaling is also in good agreement with kinetic simulations.

From the theoretical standpoint, our scaling results manifest intimate relations between boundary layers and facet evolution, which seem to remain almost intact in passing from the discrete kinetic equations to the continuum limit. The presence of the facet, where the continuum solutions develop singularities, does not cause any problems within our approach; in fact, the singular character of the slope profile near the facet is exploited here in order to determine scaling of the maximum step density for DL kinetics. Hence, our treatment transcends previously stated limitations of continuum theories.[28,33]

From the experimental standpoint, we believe that the shape profile predicted by the universal ODE, Eq. (87), for a class of axisymmetric shape profiles, or possibly its variants for non-axisymmetric profiles, may describe real experimental situations, especially those where "mounds" are created on crystalline surfaces. The coverage of nominally flat crystalline surfaces by mounds can result from homoepitaxial growth of semiconductors,[71,72] metals[73] and ceramics,[74] heteroepitaxial growth of Pb crystallites,[75] or from lithographic fabrication processes.[51] Axisymmetry is rarely observed there but two-, three-, or four-fold rotational symmetry of the mounds is frequently observed. After the completion of growth or patterning, some aspects of the relaxation of these features toward flatness at temperatures below T_R may be described by our treatment. There should be a time regime in which sufficient mass transport has occurred for the tips of the mounds to have attained a self-similar shape but insufficient mass transport has occurred to permit the tips to interact with the bases of the mounds. In this regime, profiles and scaling laws as presented here are indicative of the dependence of macroscopic features of evolution on the step energetics.

It is worthwhile placing our work in perspective with some existing treatments of surface evolution and also pointing out open questions. Our motivation for treating analytically the nanostructure decay with ratio of energy parameters $\epsilon=g_3/g_1<O(1)$ was to make direct contact with kinetic simulations.[32] Furthermore, it is necessary to develop a systematic understanding of limitations of a large body of classical work based on the original step-flow model by Burton, Cabrera and Frank[43] in which $\epsilon=0$. We emphasize that our results are consistent with the kinetic simulations although our analysis is developed within the analytical framework of continuum thermodynamics. The principal concept that emerges from our studies as a *bridge* between the two approaches is the boundary-layer idea.

In order to identify and quantify the boundary layer we considered nanostructure decays in which line tension matters, as is the case with a conical initial shape. Specifically, in

the corresponding simulations,[32] all steps including the top one move exclusively under the influence of line tension and interactions with the neighboring steps. We followed this aspect of evolution using the same interactions. Our scaling results are a direct consequence of boundary-layer theory. Specifically, we believe that the scaling of the maximum step density does not depend on the detailed form of the boundary conditions that we chose to apply.

There are features of evolution that apparently evade a precise description in our model, such as the detailed motion of the top step, which is sensitive to its kinetics and energetics. In this respect the question is raised whether suitable boundary conditions at the facet edge can be found to account for the self interaction of the top step. Mathematically, this possibility is indicated to us by the existence of the one-parameter family of similarity solutions of Sec. III [see Fig. 2(a)]; different members of this family may be reasonably "selected"[76] via boundary conditions that can incorporate different energetics, in the form of self-interaction, of the top step.

Our analysis is in the spirit of Spohn's[23] treatment of facets as free boundaries, and enriches that approach with the concept of boundary layer in order to quantify analytically the combined effect of step line tension and step-step interactions. In more technical terms, by considering a neighborhood of the facet where the slope varies appreciably, we need impose similarity only *locally* for a class of initial shapes and not globally.

A continuum aspect that needs to be explored further is the connection of the boundary-layer theory used here with the variational formulation of Ref. 30. In particular, there seems to exist an intimate relation between the nature of the boundary conditions that we apply in Sec. II C and this variational approach.

In conclusion, our continuum approach stems from familiar thermodynamic concepts and reaches analytical results by using a PDE and combining free-boundary and boundary-layer theories. It is thus promising to apply these ideas to other problems at the mesoscale and nanoscale, with or without the assumption of self-similar shapes. The extension of our studies to fine details of nanostructure decay for a range of processes may require a more careful examination of the effective boundary conditions at the facet edge.

ACKNOWLEDGMENTS

This research was supported by the Harvard NSEC. We thank N. Israeli and D. Kandel for valuable feedback and for sharing with us detailed results of their kinetic simulations to make the comparisons reported here possible. We also thank M. Z. Bazant, R. V. Kohn, and R. R. Rosales for numerous useful discussions.

APPENDIX A: ZEROTH-ORDER FACET RADIUS

In this appendix we derive Eq. (73) and also give analytical formulas for $w_0(t)$ for various initial profiles. Differentiation with respect to t of both sides of Eq. (72) gives

$$\dot{h}_{f0} = \frac{B}{w_0^3} - \frac{3Bt}{w_0^4}\dot{w}_0 + H'(w_0^+)\dot{w}_0. \tag{A1}$$

By virtue of Eq. (71), elimination of $\dot{h}_{f0}$ yields

$$\dot{w}_0 w_0^2 H'(w_0^+) = -\frac{3B}{w_0} + \frac{3Bt}{w_0^2}\dot{w}_0. \tag{A2}$$

The last equation reads

$$\frac{d}{dt}\left\{\int_{\text{const.}}^{w_0(t)} dr r^2[-H'(r)]\right\} = \frac{d}{dt}\left[\frac{3Bt}{w_0(t)}\right]. \tag{A3}$$

Integration of this equation with the initial condition $w_0(0) = W$ readily gives Eq. (73).

1. Conical initial shape

When the initial surface profile is a cone, Eq. (73) can be solved exactly for all times $t>0$. With $H'(r)=-\kappa<0$ for $r > w_0(0)=W$, $w_0(t)$ satisfies the equation

$$w_0(t)^4 - W^3 w_0(t) - \frac{9Bt}{\kappa} = 0. \tag{A4}$$

By the known procedure of finding roots of quartic polynomials,[77]

$$w_0(t) = \frac{\sqrt{u_1}}{2} + \frac{1}{2}\sqrt{2\left(u_1^2 + \frac{36Bt}{\kappa}\right)^{1/2} - u_1}, \tag{A5}$$

where

$$u_1 = s_+ - s_-, \tag{A6}$$

$$s_\pm = \left[\sqrt{\left(\frac{12Bt}{\kappa}\right)^3 + \frac{W^{12}}{4}} \pm \frac{W^6}{2}\right]^{1/3}. \tag{A7}$$

2. Long-time asymptotic formulas for class of initial shapes

We consider solutions $w_0(t)$ to Eq. (73) that, for a class of initial shapes, are monotonically increasing and unbounded for sufficiently long times t. We distinguish the following cases.

a. $Bt/w_0 \to \infty$ as $t \to \infty$

It follows that the integral in Eq. (73) diverges as $w_0 \to \infty$. We assume the slope profile

$$-H'(r) = \kappa r^\rho + \lambda r^\nu, \quad \kappa > 0, \quad \rho > \nu > -3, \tag{A8}$$

where $r > W$ and κ, λ, ρ and ν are given constants. Equation (73) furnishes

$$\kappa\frac{w_0^{\rho+4}}{\rho+3} = 3Bt - \lambda\frac{w_0^{\nu+4}}{\nu+3} + O(w_0), \tag{A9}$$

where the $O(w_0)$ terms can be neglected. The leading term for long times is

$$w_0(t) \sim \left[\frac{(\rho+3)3Bt}{\kappa}\right]^{1/(\rho+4)}. \tag{A10}$$

For $\rho=0$, an initial conical shape, this formula agrees with Eq. (A5) in the limit where $W \ll (Bt)^{1/4}$ so that $36Bt/\kappa$ dominates over u_1. The next-order term is derived from Eq. (A9) by a simple iteration:

$$w_0(t) \sim \left[\frac{(\rho+3)3Bt}{\kappa}\right]^{1/(\rho+4)} - \frac{\lambda}{\kappa}\frac{\rho+3}{(\nu+3)(\rho+4)} \times \left[\frac{(\rho+3)3Bt}{\kappa}\right]^{[1-(\rho-\nu)]/(\rho+4)}. \tag{A11}$$

In particular, for $\rho=1$ and $\nu=0$ Eq. (A8) describes a paraboloid and Eq. (A11) gives

$$w_0(t) \sim \left(\frac{12Bt}{\kappa}\right)^{1/5} - \frac{4}{15}\frac{\lambda}{\kappa}, \tag{A12}$$

in agreement with the scaling in time derived directly from the step motion in Ref. 38. If the paraboloid axis of symmetry coincides with the z-axis, then $\lambda=0$. In the case with $\lambda=0$ and arbitrary ρ, Eq. (73) gives

$$w_0(t) \sim \left[\frac{(\rho+3)3Bt}{\kappa}\right]^{1/(\rho+4)} + \frac{W^{\rho+3}}{\rho+4}\left[\frac{(\rho+3)3Bt}{\kappa}\right]^{-(\rho+2)/(\rho+4)}. \tag{A13}$$

Note that the initial facet radius, W, enters the next-order term.

The case with $\rho=-3$ and $\lambda=0$ deserves some special attention because the integral in Eq. (73) becomes logarithmically divergent. Equation (73) reads

$$\kappa w_0 \ln\left(\frac{w_0}{W}\right) = 3Bt. \tag{A14}$$

A formula for $w_0(t)$ is found by taking the logarithm of both sides of this equation:

$$w_0(t) \sim \frac{3Bt/\kappa}{\ln(3Bt/\kappa W) - \ln\ln(3Bt/\kappa W)}. \tag{A15}$$

Finally, we consider the case with $\nu=-3<\rho$ and $\lambda\neq 0$. The equation for $w_0(t)$ is

$$\kappa\frac{w_0^{\rho+4}}{\rho+3} = 3Bt - \lambda w_0 \ln\left(\frac{w_0}{W}\right) + \kappa\frac{W^{\rho+3}}{\rho+3}w_0. \tag{A16}$$

This equation is solved iteratively by treating the two last terms of its right-hand side as small:

$$w_0(t) \sim \left[\frac{(\rho+3)3Bt}{\kappa}\right]^{1/(\rho+4)} - \frac{\lambda}{\kappa}\frac{\rho+3}{\rho+4}\left[\frac{(\rho+3)3Bt}{\kappa}\right]^{-(\rho+2)/(\rho+4)} \times \ln\left\{\frac{1}{W}\left[\frac{(\rho+3)3Bt}{\kappa}\right]^{1/(\rho+4)}\right\} + \frac{W^{\rho+3}}{\rho+4}\left[\frac{(\rho+3)3Bt}{\kappa}\right]^{-(\rho+2)/(\rho+4)}. \tag{A17}$$

b. $Bt/w_0 = O(1)$ as $t\to\infty$

In this case the facet expands at a constant speed, $\dot{w}=$const. Thus, the initial slope profile must satisfy

$$I \equiv \int_W^\infty dr\, r^2[-H'(r)] < \infty. \tag{A18}$$

It follows that

$$w_0(t) \sim I^{-1}3Bt. \tag{A19}$$

In particular, when $H'(r)=-\kappa r^\rho$ and $\rho<-3$,

$$w_0(t) \sim \frac{|\rho+3|}{\kappa W^{\rho+3}}3Bt. \tag{A20}$$

The exponential slope profile $-H'(r)=\kappa e^{-\sigma r}$ $(\sigma>0)$ leads to the formula

$$w_0(t) \sim \frac{3e^{\sigma W}}{\kappa(W^2/\sigma + 2W/\sigma^2 + 2/\sigma^3)}Bt. \tag{A21}$$

The Gaussian slope profile $H'(r)=-\kappa r e^{-r^2/\alpha^2}$ gives

$$w_0(t) \sim \frac{6e^{W^2/\alpha^2}}{\kappa\alpha^2(W^2+\alpha^2)}Bt. \tag{A22}$$

APPENDIX B: SCALING FOR THE BOUNDARY-LAYER WIDTH

In this appendix we argue that Eq. (83) is the only possibility of scaling. As is common in problems of singular perturbation,[64] we assume that, to leading order in ϵ, the boundary-layer width δ scales as

$$\delta(t;\epsilon) = \epsilon^\alpha \Delta(t), \quad \alpha>0, \tag{B1}$$

where $\Delta=O(1)$ and the exponent α is to be determined. We show that there is a unique value of α consistent with the boundary condition $\mathcal{F}=0$ at $\eta=0$ and condition (79) as $\eta\to\infty$. This value can be obtained by reductio ad absurdum as described below.

By use of formula (B1), Eq. (78) reads

$$\epsilon^{3\alpha}\frac{\dot{w}\Delta^3}{B}(\mathcal{F})_\eta = \epsilon(\mathcal{F}^2)_{\eta\eta\eta\eta} + O(\epsilon^{1+\alpha}, \epsilon^{4\alpha}). \tag{B2}$$

So, we distinguish two ranges of values for α.

(i) $\alpha<\frac{1}{3}$. The leading term in Eq. (B2) is thus $O(\epsilon^{3\alpha})$; hence, $\mathcal{F}_\eta=0$, by which $\mathcal{F}(\eta,t)=0$ for all η in order to satisfy the condition of zero slope at $\eta=0$. This solution is impossible.

(ii) $\alpha>\frac{1}{3}$. The leading term in Eq. (B2) is $O(\epsilon)$. Hence, $(\mathcal{F}^2)_{\eta\eta\eta\eta}=0$, or

$$\mathcal{F}^2(\eta,t) = b_3(t)\eta^3 + b_2(t)\eta^2 + b_1(t)\eta, \tag{B3}$$

which satisfies $\mathcal{F}(0,t)=0$. So, $\mathcal{F}(\eta,t)=O(\eta^{l/2})$ as $\eta\to\infty$, where l is a positive integer, which cannot match the outer solution according to formula (79). We conclude that $\alpha=\frac{1}{3}$ is the only possible value. Futhermore, it is shown in Appendix

D that the resulting similarity solution for $\mathcal{F}$ inside the boundary layer can approach the outer solution as $\eta \to \infty$ with correction terms that decay exponentially in η.

APPENDIX C: BEHAVIOR OF $f_0(\eta)$ AS $\eta \to 0^+$

In this appendix we derive a small-η expansion for the $f_0(\eta)$ that satisfies the ODE (87) with $f_0(0)=0$. By virtue of Eq. (89) we start with the expansion

$$f_0(\eta) \sim \sum_{j=1}^{M} c_j \eta^{j/2}, \quad c_2 = 0, \quad \eta \to 0^+. \tag{C1}$$

We choose $M=11$ for the number of terms in this expansion, as a compromise between the amount of labor to calculate c_j and the accuracy needed for our actual numerical calculations. It follows that

$$\begin{aligned} f_0(\eta)^2 \sim {} & c_1^2 \eta + 2c_1c_3 \eta^2 + 2c_1c_4 \eta^{5/2} + (c_3^2 + 2c_1c_5)\eta^3 + 2(c_1c_6 \\ & + c_3c_4)\eta^{7/2} + (2c_1c_7 + 2c_3c_5 + c_4^2)\eta^4 + 2(c_1c_8 + c_3c_6 \\ & + c_4c_5)\eta^{9/2} + 2(c_1c_{10} + c_3c_8 + c_4c_7 + c_5c_6)\eta^{11/2} \\ & + (2c_1c_9 + 2c_3c_7 + 2c_4c_6 + c_5^2)\eta^5 \\ & + (2c_1c_{11} + 2c_3c_9 + 2c_4c_8 + 2c_5c_7 + c_6^2)\eta^6, \end{aligned} \tag{C2}$$

$$\begin{aligned} (f_0^2)''' \sim {} & \frac{15}{4}c_1c_4\eta^{-1/2} + 6(c_3^2 + 2c_1c_5) + \frac{105}{4}(c_1c_6 + c_3c_4)\eta^{1/2} \\ & + 24(2c_1c_7 + 2c_3c_5 + c_4^2)\eta + \frac{315}{4}(c_1c_8 + c_3c_6 \\ & + c_4c_5)\eta^{3/2} + 60(2c_1c_9 + 2c_3c_7 + 2c_4c_6 + c_5^2)\eta^2 \\ & + \frac{693}{4}(c_1c_{10} + c_3c_8 + c_4c_7 + c_5c_6)\eta^{5/2} + 120(2c_1c_{11} \\ & + 2c_3c_9 + 2c_4c_8 + 2c_5c_7 + c_6^2)\eta^3. \end{aligned} \tag{C3}$$

From Eq. (87), the last expansion equals

$$f_0 - 1 \sim -1 + c_1\eta^{1/2} + c_3\eta^{3/2} + c_4\eta^2 + c_5\eta^{5/2} + c_6\eta^3. \tag{C4}$$

The system of equations for the coefficients thus is

$$c_4 = 0, \quad 6(c_3^2 + 2c_1c_5) = -1, \quad \frac{105}{4}(c_1c_6 + c_3c_4) = c_1,$$

$$24(2c_1c_7 + 2c_3c_5 + c_4^2) = 0, \quad \frac{315}{4}(c_1c_8 + c_3c_6 + c_4c_5) = c_3,$$

$$60(2c_1c_9 + 2c_3c_7 + 2c_4c_6 + c_5^2) = c_4,$$

$$\frac{693}{4}(c_1c_{10} + c_3c_8 + c_4c_7 + c_5c_6) = c_5,$$

$$120(2c_1c_{11} + 2c_3c_9 + 2c_4c_8 + 2c_5c_7 + c_6^2) = c_6. \tag{C5}$$

After some algebra the coefficients c_j for $j \geqslant 5$ are calculated in terms of c_1 and c_3 (recall that $c_2 = c_4 = 0$),

$$c_5 = -\frac{1}{2c_1}\left(c_3^2 + \frac{1}{6}\right), \quad c_6 = \frac{4}{105},$$

$$c_7 = \frac{c_3}{2c_1^2}\left(c_3^2 + \frac{1}{6}\right), \quad c_8 = -\frac{8}{315}\frac{c_3}{c_1},$$

$$c_9 = -\frac{5}{8c_1^3}\left(c_3^2 + \frac{1}{30}\right)\left(c_3^2 + \frac{1}{6}\right),$$

$$c_{10} = \frac{4}{55c_1^2}\left(\frac{4c_3^2}{7} + \frac{1}{27}\right),$$

$$c_{11} = \frac{c_3}{4c_1^4}\left(c_3^2 + \frac{1}{6}\right)\left(\frac{7c_3^2}{2} + \frac{1}{4}\right) + \frac{202}{(105)^2 c_1}. \tag{C6}$$

APPENDIX D: BEHAVIOR OF $f_0(\eta)$ AS $\eta \to \infty$

In this appendix we derive an asymptotic formula when η is large for the $f_0(\eta)$ that satisfies Eq. (87) with $f_0(\infty)=1$. Because of condition (86) we introduce a function $g_0(\eta)$ such that

$$f_0(\eta) = 1 + g_0(\eta), \quad |g_0| \ll 1, \quad \eta \gg 1. \tag{D1}$$

Substitution of this formula into Eq. (87) yields the ODE

$$2g_0''' - g_0 = O(g_0^2). \tag{D2}$$

By neglecting the right-hand side of this equation, we notice that the resulting linear ODE has three independent solutions, one of which is a growing exponential:

$$g_0(\eta) \sim Ce^{2^{-1/3}\eta} + Ae^{-2^{-4/3}\eta}\cos\left(\frac{\sqrt{3}}{2^{4/3}}\eta + \phi\right), \tag{D3}$$

where A, C and ϕ are arbitrary real constants. We thus take $C=0$ in order to suppress the growing exponential. The resulting formula is

$$g_0(\eta) \sim Ae^{-2^{-4/3}\eta}\cos\left(\frac{\sqrt{3}}{2^{4/3}}\eta + \phi\right), \quad \eta \gg 1. \tag{D4}$$

[1] H.-C. Jeong and E. D. Williams, Surf. Sci. Rep. **34**, 171 (1999).
[2] H. P. Bonzel, Prog. Surf. Sci. **67**, 45 (2001).
[3] W. K. Burton and N. Cabrera, Discuss. Faraday Soc. **5**, 33 (1949).
[4] M. Wortis, in *Fundamental Problems in Statistical Mechanics VI*, edited by E. G. D. Cohen (North-Holland, Amsterdam, 1985), pp. 87–123.
[5] H. van Beijeren and I. Nolden, in *Structure and Dynamics of Surfaces II*, edited by W. Schommers and P. von Blanckenhagen (Springer, Berlin, 1987), pp. 259–300.
[6] P. Nozières, in *Solids Far from Equilibrium*, edited by C. Godreche (Cambridge U. P., Cambridge, 1992), pp. 1–154.
[7] P. Nozières, Eur. Phys. J. B **24**, 383 (2001).
[8] In principle, crystal facets have constant slope which may or may not be zero. In this paper the slope along the facet is taken to be zero without loss of generality.
[9] A. Pimpinelli and J. Villain, *Physics of Crystal Growth* (Cambridge U. P., Cambridge, 1998), Chap. 1.
[10] E. D. Williams, Surf. Sci. **299**, 502 (1994).
[11] Z. Suo, Adv. Appl. Mech. **33**, 193 (1997).
[12] W. W. Mullins, J. Appl. Phys. **28**, 333 (1957).
[13] W. W. Mullins, J. Appl. Phys. **30**, 77 (1959).
[14] C. Herring, in *Physics of Powder Metallurgy*, edited by W. E. Kingston (McGraw-Hill, New York, 1951).
[15] C. Herring, Phys. Rev. **82**, 87 (1951).
[16] E. E. Gruber and W. W. Mullins, J. Phys. Chem. Solids **28**, 875 (1967).
[17] H. P. Bonzel, E. Preuss, and B. Steffen, Appl. Phys. A: Solids Surf. **35**, 1 (1984); Surf. Sci. **145**, 20 (1984).
[18] E. Preuss, N. Freyer, and H. P. Bonzel, Appl. Phys. A: Solids Surf. **41**, 137 (1986).
[19] A. Rettori and J. Villain, J. Phys. (France) **49**, 257 (1988).
[20] F. Lancon and J. Villain, in *Kinetics of Ordering and Growth at Surfaces*, edited by M. Lagally (Plenum, New York, 1990).
[21] M. Ozdemir and A. Zangwill, Phys. Rev. B **42**, 5013 (1990).
[22] J. Stewart and N. Goldenfeld, Phys. Rev. A **46**, 6505 (1992).
[23] H. Spohn, J. Phys. I **3**, 69 (1993).
[24] J. Hager and H. Spohn, Surf. Sci. **324**, 365 (1995).
[25] H. P. Bonzel and E. Preuss, Surf. Sci. **336**, 209 (1995).
[26] H. P. Bonzel and W. W. Mullins, Surf. Sci. **350**, 285 (1996).
[27] M. V. R. Murty, Phys. Rev. B **62**, 17 004 (2000).
[28] N. Israeli and D. Kandel, Phys. Rev. Lett. **88**, 116103 (2002).
[29] D. Margetis, M. J. Aziz, and H. A. Stone, Phys. Rev. B **69**, 041404(R) (2004).
[30] V. B. Shenoy and L. B. Freund, J. Mech. Phys. Solids **50**, 1817 (2002).
[31] A. Chame, S. Rousset, H. P. Bonzel, and J. Villain, Bulg. Chem. Commun. **29**, 398 (1996).
[32] N. Israeli and D. Kandel, Phys. Rev. B **60**, 5946 (1999).
[33] N. Israeli and D. Kandel, Phys. Rev. B **62**, 13 707 (2000).
[34] M. V. R. Murty and B. H. Cooper, Phys. Rev. B **54**, 10 377 (1996).
[35] M. A. Dubson and G. Jeffers, Phys. Rev. B **49**, 8347 (1994).
[36] Z. Jiang and C. Ebner, Phys. Rev. B **40**, 316 (1989).
[37] J. D. Erlebacher and M. J. Aziz, Surf. Sci. **374**, 427 (1997).
[38] M. Uwaha, J. Phys. Soc. Jpn. **57**, 1681 (1988).
[39] C. Duport, A. Chame, W. W. Mullins, and J. Villain, J. Phys. I **6**, 1095 (1996).
[40] E. Adam, A. Chame, F. Lancon, and J. Villain, J. Phys. I **7**, 1455 (1997).
[41] N. Israeli and D. Kandel, Phys. Rev. Lett. **80**, 3300 (1998).
[42] N. Israeli, H.-C. Jeong, D. Kandel, and J. D. Weeks, Phys. Rev. B **61**, 5698 (2000).
[43] W. K. Burton, N. Cabrera, and F. C. Frank, Philos. Trans. R. Soc. London, Ser. A **243**, 299 (1951).
[44] G. Ehrlich and F. Hudda, J. Chem. Phys. **44**, 1039 (1966).
[45] R. L. Schwoebel and E. J. Shipsey, J. Appl. Phys. **37**, 3682 (1966).
[46] Equation (1) should always hold in the continuum limit regardless of the specifics of the limit procedure. If $\mathbf{j}(\mathbf{r},t)$ is not differentiable in some region $\mathcal{R}$, Eq. (1) is interpreted in terms of a "weak" formulation via integration over an area in the neighborhood of $\mathcal{R}$.
[47] This approximation is not expected to hold for $i=1$, i.e., for the top layer bounded by the first step, at the late stages of the top step collapse.
[48] G. S. Bales and A. Zangwill, Phys. Rev. B **41**, 5500 (1990).
[49] By the symbol $\sim$ here we mean that the two sides of the corresponding relation become equal in some sense in the limit under consideration.
[50] J. Tersoff, M. D. Johnson, and B. G. Orr, Phys. Rev. Lett. **78**, 282 (1997).
[51] S. Tanaka, N. C. Bartelt, C. C. Umbach, R. M. Tromp, and J. M. Blakely, Phys. Rev. Lett. **78**, 3342 (1997).
[52] Note the discrepancy between the second term on the right-hand side of our Eq. (7), which has the form of the divergence in $\mathbf{r}_i = r_i\hat{\mathbf{e}}_r$, $\nabla_i\cdot((V/2\pi r_i)\hat{e}_r)$, and the corresponding term of Eq. (8) in Ref. 32, which involves simply the derivative in r_i, $(\partial/\partial r_i)(V/2\pi r_i)$. As a result, our formulas for μ_i and its continuum counterpart $\mu(r,t)$, Eqs. (9) and (26) here, respectively, differ from the corresponding Eqs. (9) and (31) in Ref. 32. We believe that our Eq. (7) is consistent with the definition of V in Ref. 51, whereas Eq. (8) in Ref. 32 is not.
[53] This condition is not expected to hold for $i=0$, which corresponds to the top step.
[54] D. Margetis (unpublished).
[55] N. Cabrera, Surf. Sci. **2**, 320 (1964).
[56] C. Jayaprakash, C. Rottman, and W. F. Saam, Phys. Rev. B **30**, 6549 (1984).
[57] R. Najafabadi and D. Srolovitz, Surf. Sci. **317**, 221 (1994).
[58] A. F. Andreev, Zh. Eksp. Teor. Fiz. **80**, 2042 (1981).
[59] We always assume that evolution occurs near equilibrium.
[60] Our definition of $\mathbf{N}$ here differs from the one in Ref. 29 where $\mathbf{N}=-(\partial G/\partial h_x, \partial G/\partial h_y)$.
[61] V. B. Shenoy, A. Ramasubramaniam, H. Ramanarayan, D. T. Tambe, W-L. Chan, and E. Chason, Phys. Rev. Lett. **92**, 256101 (2004); these authors have derived the same PDE for the height profile independently via postulating relation (30).
[62] In Ref. 32 the authors use the condition $F=0$ at $r=w$ for long times, when their similarity solution is valid. In our approach the same condition is imposed at all times $t>0$.
[63] C. Jayaprakash, W. F. Saam, and S. Teitel, Phys. Rev. Lett. **50**, 2017 (1983).
[64] E. J. Hinch, *Perturbation Methods* (Cambridge U. P., Cambridge, 1991), Chap. 5.
[65] A precise condition on the time t for the validity of the similarity form (80) should also account for the constraint $\delta \ll w$, which is needed for applying boundary-layer theory. For a class of initial shapes, the time t may not be arbitrarily long as δ may increase faster than w; in this case $\delta \sim w$ at times monotonically decreasing in ϵ.

[66] We assume that, within our continuum theory, the facet local radius of curvature is a smooth and (sufficiently) slowly varying function of the arc length.

[67] From the standpoint of the first-order kinetic (discrete) equations of Sec. II A, the step density $F_i = a/(r_{i+1} - r_i)$ becomes small, yet remains nonzero, for large step separation distances, as is the case in the vicinity of the top step; the ADL kinetics dominate at distances where $mF_i \gg 1$.

[68] N. Israeli and D. Kandel, private communication (2003).

[69] Work on the continuum limit for ADL kinetics is in progress.

[70] In Ref. 32 the authors do not take into account the Ehrlich-Schwoebel barrier; so we can trivially take $k_u = k_d$ in Eq. (3) for complete analogy with their formulation.

[71] M. D. Johnson, C. Orme, A. W. Hunt, D. Graff, J. Sudijono, L. M. Sander, and B. G. Orr, Phys. Rev. Lett. **72**, 116 (1994).

[72] J. E. Van Nostrand, S. J. Chey, and D. G. Cahill, Phys. Rev. B **57**, 12 536 (1998).

[73] J.-K. Zuo and J. F. Wendelken, Phys. Rev. Lett. **78**, 2791 (1997).

[74] B. W. Karr, I. Petrov, D. G. Cahill, and J. E. Greene, Appl. Phys. Lett. **70**, 1703 (1997).

[75] K. Thürmer, J. E. Reutt-Robey, E. D. Williams, M. Uwaha, A. Emundts, and H. P. Bonzel, Phys. Rev. Lett. **87**, 186102 (2001).

[76] "Selection" of a similarity solution here means that the requisite ODE is solved uniquely via supplying boundary conditions that effectively account for the motion of the first few steps at long times, possibly without resort to kinetic simulations. Hence, the selection here does not mean to require the passage to early times and the fine details of the initial conditions.

[77] G. Birkhoff and S. Mac Lane, *A Survey of Modern Algebra* (MacMillan, New York, 1959), pp. 112–115.